TRANSPORT-CONTROLLING NANOSCALE MULTILAYERS FOR BIOMEDICAL DEVICES

A Dissertation

by

JAE BUM PARK

Submitted to the Office of Graduate Studies of
Texas A&M University
in partial fulfillment of the requirements for the degree of

DOCTOR OF PHILOSOPHY

August 2012

Major Subject: Materials Science and Engineering

Transport-Controlling Nanoscale Multilayers for Biomedical Devices

TRANSPORT-CONTROLLING NANOSCALE MULTILAYERS FOR BIOMEDICAL DEVICES

A Dissertation

by

JAE BUM PARK

Submitted to the Office of Graduate Studies of
Texas A&M University
in partial fulfillment of the requirements for the degree of

DOCTOR OF PHILOSOPHY

Approved by:

Chair of Committee,	Michael J. McShane
Committee Members,	Jun Kameoka
	Haiyan Wang
	Mustafa Akbulut
Intercollegiate Faculty Chair,	Ibrahim Karaman

August 2012

Major Subject: Materials Science and Engineering

ABSTRACT

Transport-Controlling Nanoscale Multilayers for Biomedical Devices.

(August 2012)

Jae Bum Park, B.S., Hallym University; M.S., Hallym University

Chair of Advisory Committee: Dr. Michael J. McShane

Recent advances in multilayer self-assembly have enabled the precise construction of nanocomposite ultrathin films on a variety of substrates, from large-area planar surfaces to nanoparticles. As a result, a wide range of physico-chemical properties may be represented by selecting from an array of surface preparations, molecules, assembly conditions, and post-assembly treatments. Such multilayer nanofilm assemblies are particularly attractive for use as specialized membranes for selective transport, which have many applications for separations, sensors, and drug delivery systems.

In this work, nanocomposite ultrathin films built with layer-by-layer (LbL) self-assembly methods have been applied to surface modification to control interfacial behavior, including diffusion, anti-fouling, and biomimetic membranes. Transport and interfacial properties of nanocomposite membranes constructed using LbL self-assembly with synthetic and/or bio-polymers were characterized, and permeability values of clinically relevant small molecules through the nanofilms were determined. Correlations between permeability and film properties were also examined.

Nanofilm coatings around 100nm thickness decreased diffusion coefficients of glucose up to five orders of magnitude, and were found to greatly affect enzymatic glucose sensor responses. Surface modification on top of the nanofilms with poly(ethylene glycol) provided anti-fouling effects. However, weak-weak polyelectrolyte multilayers (PEMs) should not be used to control transport due to their susceptibility under normal physiological conditions. Natural/biological polymers also provided multilayer film structures at the specific conditions, but their transport-limiting properties were not significant compared to synthetic PEMs. Even when covalently crosslinked, biological PEMs did not reduce the permeability of a small molecule. Finally, the predicting model of projecting analyte permeation through multi-phase nanocomposite films comprised with known diffusion coefficients was theoretically and experimentally evaluated. The modeling was matched reasonably well to experimental data.

The outcomes will be the key knowledge or engineering principles to support future efforts in research and development. It is anticipated that the system developed for determining transport properties will provide a general platform for assessing new candidate materials. The theory developed will be useful in estimating transport properties of novel nanocomposite materials that may be interesting in a broad array of chemical and biological systems, from analytical separations to implantable biomedical applications, and will provide useful design rules for materials and fabrication process selection.

ACKNOWLEDGEMENTS

I would never have been able to finish my dissertation without the guidance of my committee members, help from colleagues, and support from my family and wife.

First and foremost, I would like to express my utmost gratitude to my advisor, Dr. Mike McShane, for his excellent guidance, caring, patience, and providing me an excellent atmosphere for doing research.

I also would like to thank my committee members, Dr. Kameoka, Dr. Wang, and Dr. Akbulut for their guidance and support throughout the course of this research.

Thanks to my friends and colleagues, Dustin Ritter, Brad Collier, Jason Roberts, Ashvin Nagaraja, Merene Philip, Rachel Unruh, Dr. Saurabh Singh, and Dr. Ruiqi Long. Thanks also to department faculty and staff for making my time at Texas A&M University a great experience. I also want to extend my gratitude to the National Science Foundation, which provided financial support for this research.

Finally, thanks to my mother and father for their encouragement and to my wife for her patience and love.

NOMENCLATURE

LbL	Layer-by-layer
PEM	Polyelectrolyte multilayer
BPEM	Biopolyelectrolyte multilayer
D	Diffusion coefficient
C_0	Initial concentration
C_1	Feed concentration
C_2	Permeate concentration
C_m	Membrane concentration
A	Area of the nanofilm
V	Volume of liquid chamber
l	Length of the liquid chamber
L	Thickness of the nanofilm
Φ	Partition coefficient
PSS	Poly(styrene sulfonate)
PAA	Poly(acrylic acid)
PAH	Poly(allylamine hydrochloride)
PLL	Poly(L-lysine)
PEG	Poly(ethylene glycol)
Alg	Alginic acid
Chi	Chitosan

Hep	Heparin
DS	Dextran sulfate
PGA	Poly(L-glutamic acid)

TABLE OF CONTENTS

Page

Page

Page

LIST OF FIGURES

Page

Page

Page

Page

Page

LIST OF TABLES

Page

1. INTRODUCTION: SIGNIFICANCE AND BACKGROUND*

Implanted medical devices require proper interfacial materials which play key roles, especially when enzymatic systems are involved. There are three special requirements that must be considered carefully in selecting materials. First, a suitable matrix for immobilization of the biological elements must be identified and a suitably gentle process for construction of the enzyme phase must be developed. Second, a transport-limiting membrane, often a coating applied to the reactive enzyme phase, must be employed. This enables the appropriate balance between the diffusion of substrate(s) to the enzyme and the consuming reaction, such that a depletion of substrate or local increase of product that is proportional to the target analyte concentration can be realized.[1] Third, surface fouling and host response to foreign materials initiated by protein adsorption must be minimized while maintaining control over the transport of molecules into the implant.[2, 3] Masking implants to avoid protein adsorption enhances biocompatibility and minimizes fouling of surfaces which may alter substrate flux, shifting sensor response profiles.

Recent advances in multilayer self-assembly have enabled the precise construction of nanocomposite ultrathin films on a variety of substrates, from large-area planar surfaces to nanoparticles.[4] As a result, a wide range of physico-chemical

---

This dissertation follows the style of *ACS Applied Materials & Interfaces*.

properties may be represented by selecting from an array of surface preparations, molecules, assembly conditions, and post-assembly treatments. Such multilayer nanofilm assemblies are particularly attractive for use as specialized membranes for selective transport, which have many applications for separations and sensors. In particular, chemical sensors which rely on measurements of enzymatic reaction require precise control over the reaction and diffusion rates. Through such control, it is possible to achieve an appropriate balance of consumption and replenishment of the measurement and to tune the sensitivity and range of the response to the analyte.

Self-assembly provides a unique opportunity to realize functional systems at the micro/nanoscale. In particular, layer-by-layer (LbL) self-assembly is a technique that holds great promise for realization of biosensors due to the mild aqueous conditions, versatility in materials, and high precision.[4-6] The assembly process, illustrated in Figure 1, is facile and allows precise formation of films with total thickness of 1 nm to micrometer scale, composed of many layers containing alternately charged molecules, on any charged substrate—from planar surfaces to colloids. The thickness of individual layers is on the order of 1 nm.[7] This idea is extremely general and implies that there is no principal restriction on the choice of adsorbing species other than sufficient charge to create multiple ionic bonds to anchor the molecules to the substrate. The technique has been applied successfully to many polyions and dyes,[8-12] for the assembly of organized protein multilayers,[10] and charged nanoparticles.[8, 12] Furthermore, the LbL process has been demonstrated for applications in bionanoreactors[13] and sensors.[10, 14, 15] It has been

shown that enzymatic activity of enzymes is preserved and protected from degradation in multilayers with polyions.[16]

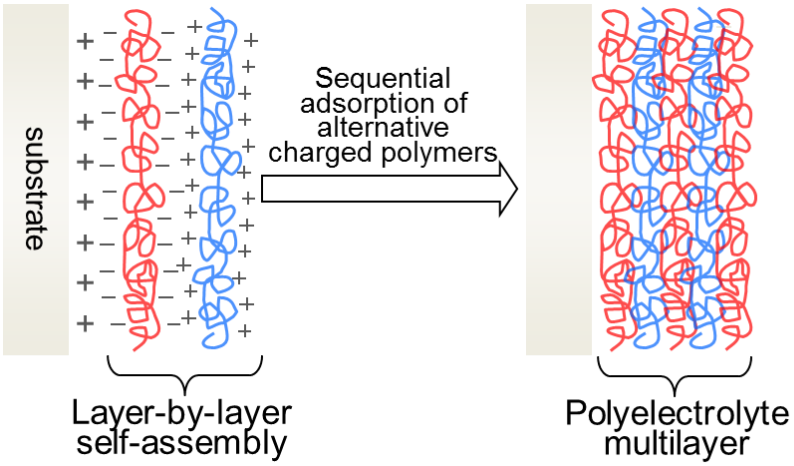

Figure 1. Schematic diagram of diffusion-limiting layer-by-layer self-assembled polyelectrolyte multilayer. Sequential electrostatic interaction between oppositely-charged polyelectrolytes on any charged substrate.

In the world of enzymatic biosensors, glucose sensors have emerged as prime examples of this technology, where typical devices operate based on the oxidation of glucose driven by glucose oxidase (GOx).[17] However, physiological glucose levels are 2.3-23 mM (supplied via diffusion from capillaries) while oxygen levels range from 0-277 μM (supplied via diffusion from the atmosphere and diffusion from capillaries);[18-20] under these conditions, membranes of low relative glucose diffusivity are required to balance oxygen and glucose transport to obtain a glucose-limited response. A wide variety of materials have been proposed to provide this control, including

poly(dimethylsiloxane) (PDMS),[21, 22] Nafion,[23-26] nanoporous silicon membranes,[27] and polyethylene-*block*-polystyrene.[28]

Although these materials have performed well in macroscale sensors, the options for transport-controlling coatings become very limited when materials amenable to self-assembly are required, such as for devices with all dimensions at a scale where individual manipulation is impractical (e.g., microspheres, nanoparticles). When attempting to shrink the size of biosensors to the level that self-assembly is used to fabricate the devices, two major difficulties arise for the choice of materials. First, achieving the necessary balance of diffusion and reaction becomes increasingly difficult because the overall diffusion lengths are extraordinarily small; thus, membranes that provide even lower diffusivity are required. Second, the selection of materials depends on the methods used for fabrication, and this immediately rules out certain classes of materials, because there are no suitable approaches to deposit these materials with micro/nanoscale precision on the enzyme-included matrices.

An attractive possibility to construct such transport-limiting coatings is the layer-by-layer (LbL) self-assembly technique, due to the flexibility of the approach to create composite films with nanometer resolution of thickness.[4, 6] Bruening *et al.* published a series of reports describing the transport of various molecular species through PEMs.[29-31] They demonstrated that the glucose diffusivity through "model" PEMs was up to four orders of magnitude smaller than glucose diffusivity in water.[29] Exploiting this extraordinarily low glucose diffusivity and precision for assembly, McShane and co-

workers have successfully applied LbL films as tunable diffusion-limiting coatings for optical biosensors.[32, 33]

To construct the transport barrier for biosensors, one must consider a set of parameters, which include the size of sensors, enzyme concentration, reaction scheme, analyte concentration, and a combination of thickness and diffusion coefficient for a given sensor interior matrix. The goal of such coordination is to maximize sensitivity while ensuring diffusion-limited behavior over the range of interest when biosensor applications are considered. In most electrochemical biosensors, LbL systems have been employed only for the immobilization of enzyme or inclusion of active redox elements.[34, 35] The diffusion properties of polyelectrolyte multilayers (PEMs) constructed by LbL self-assembly become attractive choices from available materials. Previous uses of these materials for biosensing and transport-control have been confined to a very limited set of film components and permeating species as discussed earlier (e.g. PDMS, Nafion, nanoporous silicon membrane, and block copolymer). While the potential value of PEMs in producing novel coatings for many applications is obvious, the ability to engineer films with desired functionality is limited by the current understanding of fundamental properties.

Based on previous published work and survey of available information, we established an infrastructure for construction and measurement of transport-controlling materials that can be used for biomedical applications. This dissertation is composed of five main sections discussing: (1) exploring the diffusion of target analytes through self-assembled, nanoscale multilayer films and correlating this with the film composition; (2)

advancing biosensor development by applying improved transport-limiting membranes to sensor systems; (3) modifying diffusion-limiting film surface with protein-resistance; (4) expanding the material selection in biological polymers such as natural materials, polypeptides, and polysaccharides; and (5) integrating and predicting multi-phase nanocomposite films based on all the known properties of individual components.

2. PROPERTIES OF DIFFUSION-LIMITING POLYELECTROLYTE MULTILAYERS CONSTRUCTED BY LAYER-BY-LAYER SELF-ASSEMBLY*

2.1. Introduction

Transport-limiting coatings constructed by layer-by-layer (LbL) self-assembly technique can create nanoscale composite films.[4, 6] As we discussed in Section 1, Bruening *et al.* published a series of reports describing the transport of various molecular species through PEMs.[29-31] In one report, the transport of uncharged solutes such as glucose, glycerol, and sucrose through PEMs with various film architectures was explored, and results demonstrated that the glucose diffusivity through "model" PEMs (9.87×10^{-10} cm^2/sec) was four orders of magnitude smaller than glucose diffusivity in water (6.9×10^{-6} cm^2/sec).[29]

In this Section, we describe the construction of a novel experimental system to extract diffusion coefficients for the small molecules of interest through multilayer nanofilms. Film deposition was validated by various instrumental analysis, and diffusion coefficient of glucose through PEMs was determined with establishing a general theory of film permeabilities. We expanded the application space to additional clinical-relevant biomolecules and substrates as analytes in enzyme reactions that

---

possess different sizes and charges. We selected urea (MW 60g/mol) and L-lactate (MW 90g/mol) in addition to the glucose (MW 180g/mol), since most clinical-relevant biomolecules less than 1,000 Dalton are neutral or anionic under physiological environment (Figure 4). Diffusion coefficients (*D*) of individual molecules through multilayers of most well-studied materials such as poly(styrene sulfonate) (*PSS*) and poly(allylamine hydrochloride) (*PAH*) were determined (Figure 3), and *D* values from a mixture of all analyte solutions (glucose, urea, and lactate were in one feed solution) were also measured.

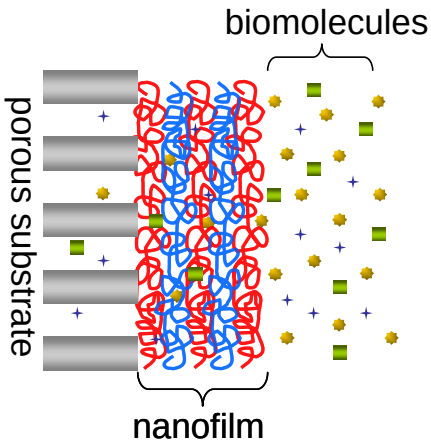

Figure 2. Schematic of diffusion-limiting nanofilm coatings on a porous substrate in the presence of various biomolecules.

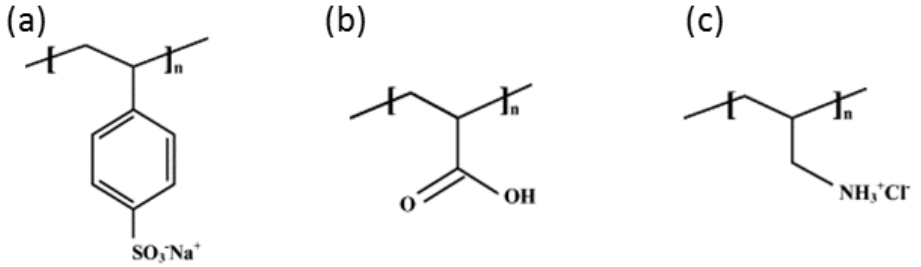

Figure 3. Molecular structures of PSS (a), PAA (b), and PAH (c).

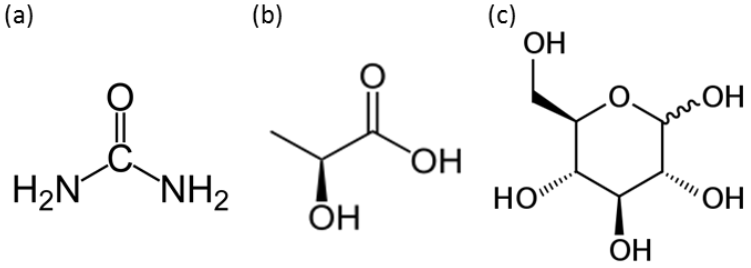

Figure 4. Molecular structures of urea (a), lactate (b), and glucose (c).

2.2. Materials and Methods

2.2.1. Materials

Poly(styrene sulfonate) (*PSS*, M_w~70,000, strong polyanion), poly(acrylic acid) (*PAA*, M_w~100,000, 35 wt. % in water, weak polyanion, *pKa*~6.2)[36], poly(allylamine

hydrochloride) (*PAH*, M_w~70,000, weak polycation, *pKa*~8.5)[37], and poly(ethyleneimine) (*PEI*, M_n~60,000, 50 wt. % in water) were purchased from Aldrich. Glucose, urea, sodium L-lactate, glucose oxidase, peroxidase, *o*-dianisidine, NaCl, NaOH, HCl, and phosphate-buffered saline (PBS) were purchased from Sigma. The porous alumina supports (Anodisc 25, 0.02 μm pore diameter) were purchased from Whatman Ltd. Deionized water (>18.2 MΩcm) was always used for preparation of polyelectrolyte solutions and rinsing. The pH of the polyelectrolyte solutions was adjusted with either HCl or NaOH.

2.2.2. Layer-by-Layer (LbL) self-assembly of nanofilms

In LbL assembly, both a sufficient amount of salt and optimum pH are required to preserve ionic strength of polyelectrolytes (especially for weak polyelectrolytes). Our film deposition of PSS/PAH fukms followed previously reported methods [29-31]. Assembly started with exposure of one side of the alumina support using open-face filter holders (Pall Co.) in 0.02M PSS in 0.5M NaCl solution adjusted to pH 2.1 for 5 min. The alumina support was rinsed with deionized water for 1 min before exposure to 0.02M PAH in 0.5M NaCl adjusted to pH 2.3 for 5 min, followed by another water rinse for 1 min. PAA/PAH alternative adsorption involved same deposition and rinse time with 0.02M PAA (pH 5.5, 0.5 M NaCl) and 0.02M PAH (pH 5.5, 0.5 M NaCl). This process was repeated until the target number of layers was achieved.

2.2.3. Nanofilm characterization

The nanofilm assemblies and key properties of the films (i.e. film morphology, real-time mass uptake, surface wettability, and thickness) were characterized by scanning electron microscope (SEM, Quanta 600 FE-SEM, FEI Company) and quartz crystal microbalance (QCM, QCM200, Stanford Research Systems, Inc.). LbL process was monitored using QCM. Each solution of polyelectrolytes described in Section *2.2.2.* was alternatively introduced for 30 min into the flow system after rinsing and stabilizing the QCM frequency until the desired number of layer was reached. Frequency shifts were measured before, during, and after exposure to polyelectrolytes, and measurements were performed under continuous flow at 50 µl/min. Static (θ_{static}) contact angle (*CA*) measurements of deionized water droplets at the nanofilm-air interface were measured by goniometer (CAM200, KSV Instruments, Ltd.) at room temperature. Thickness and refractive index were measured by ellipsometry (EP3-SE, Nanofilm, Inc.) in a four-zone compensator mode to minimize errors in surface homogeneity. For all thickness and refractive index measurements, we prepare at least three different films with same composition, and measure the thickness and refractive indices at five different locations on each film surface. Thus, reported values are average and 95% confidence intervals of n=15 different measurements.

2.2.4. Diffusion measurements

Three parallel horizontal diffusion cells (Permegear, Inc.) were used to study the transport of target molecules through the polyelectrolyte nanofilms. Each cell consists of two parts which are feed and permeate chambers. The alumina support, coated with the film of interest, was placed in between the chambers. The permeate chamber was filled with PBS, and the feed chamber contained 0.4 mM glucose in PBS. At this time, a drive with a high-precision multi-channel pump withdrew liquid synchronously from both feed and permeate chambers to maintain constant volume, and temperature of the diffusion cells was maintained by water circulator at 25 °C. All diffusion measurements ran separately with at least three nanofilms with same composition for statistical purposes. Once diffusion coefficients are determined by experiments conducted at room temperature, we can predict the diffusion coefficients at different temperature based on Einstein-Stokes equation ($D = {K_B T}/{6\pi\eta r}$). Based the difference of D values between room temperature and 37°C is only 3% by assuming all parameters other than temperature are independent of the temperature.

The sampled permeate solution was transferred to a 96-well plate through the fraction collector. All operations were performed with control provided by a computer running custom LabVIEW virtual instrumentation. Glucose concentration was measured by plate reader (Infinite F200, Tecan, Ltd.) after 30 min of incubation at 37 °C with an added reaction mixture of glucose oxidase, peroxidase, and *o*-dianisidine.[38] The

concentrations of both urea and lactate from the permeate solution were analyzed using either electrochemical biochemistry analyzer or micro-plate reader.

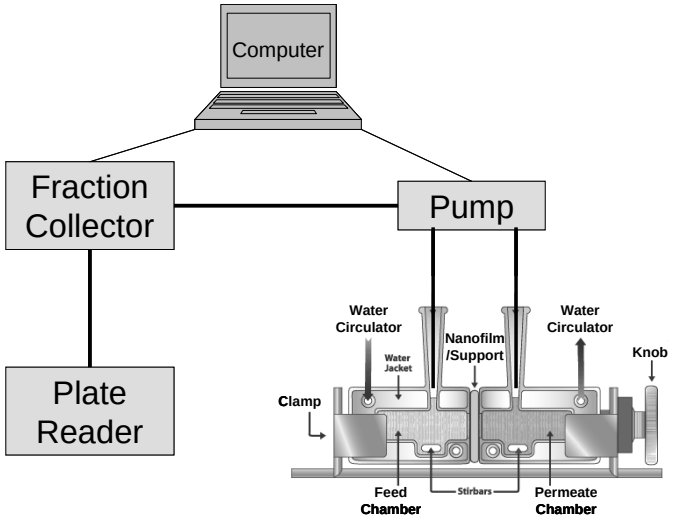

Figure 5. Automated experimental design to determine the diffusion coefficients of target molecules through nanofilms

2.2.5. Calculation of diffusion coefficients

Using the experimentally-obtained permeate concentration profile, analyte diffusion coefficient through the substrate may be determined by regression of flux and concentration gradient data using *Fick's first law.* This technique has been successfully applied to similar systems.[39]

Terms are defined by the following:

C_0 : the initial concentration

C_1 : the feed concentration

C_2 : the permeate concentration

C_m : the analyte concentration in membrane

A : the area of the nanofilm

V : the volume of liquid chamber

l : the length of the liquid chamber

L : the thickness of the nanofilm

Φ : the partition coefficient.

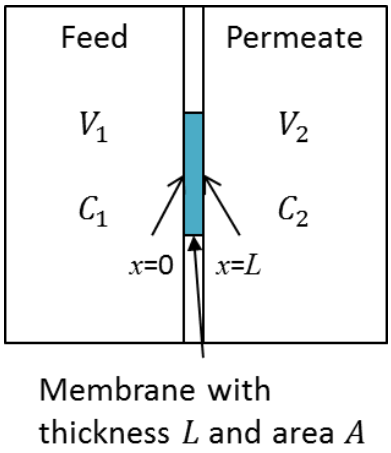

Figure 6. Diffusion of small molecules through nanocomposite membrane model.

Assuming no chemical reaction between analyte and membrane

$$\frac{dC}{dt} = 0 = D\frac{d^2C_m}{dx^2}$$

Boundary conditions are

$$x = 0, \quad C_m = \Phi C_0$$

$$x = L, \quad C_m = \Phi C_L$$

General solution is

$$C_m = Ax + B$$

Application of boundary condition yields

$$x = 0, \quad \Phi C_0 = B$$

$$x = L, \quad \Phi C_L = AL + \Phi C_0$$

$$A = -\frac{\Phi(C_0 - C_L)}{L}$$

The resulting concentration is

$$C_m = \Phi C_0 - \Phi(C_0 - C_L)\frac{x}{L}$$

From the definition of diffusive flux

$$J = -D\frac{dC_m}{dx} = \frac{D\Phi}{L}(C_0 - C_L)$$

Mass balance applied to the solute on both side of membrane

[moles of solute leaving feed/unit time] = [moles of solute transported across membrane]

The number of moles transported across the membrane per unit time is simply the product of the flux and area

$$-V_1 \frac{dC_1}{dt} = A_m D_m \Phi \frac{(C_1 - C_2)}{L}$$

To integrate this expression, the concentrations $C_1 \; and \; C_2$ must be related. This is done by noting that after the solute leaves side 1, either it is in the membrane or it is on side 2. The loss of solute from side 1 is balanced by the gain of solute in the membrane or on side 2; that is,

$$-V_1 \frac{dC_1}{dt} = -\left(\frac{V_m}{\Phi}\frac{dC_m}{dt} + V_2 \frac{dC_2}{dt}\right)$$

If $V_1 = V_2 = V$ and $V_m \ll V$, then the first term on the right-hand side is much less than the other two terms. This means that the amount of solute in the membrane is small relative to the amount of solute in either reservoir. As a result, above equation can be simplified to

$$\frac{dC_1}{dt} = -\frac{dC_2}{dt}$$

Using the initial conditions $C_1 = C_0 \; and \; C_2 = 0$, we can integrate above equation to yield

$$C_1 - C_0 = -C_2 \; or \; C_2 = C_0 - C_1$$

Substituting equation into above equation:

$$-V_1 \frac{dC_1}{dt} = A_m D_m \Phi \frac{(2C_1 - C_0)}{L}$$

$$C_2 = \frac{AD\Phi t(C_0 - 2C_2)}{VL} = \frac{D\Phi t(C_0 - 2C_2)}{lL}$$

$$D = \frac{dC}{dt}\frac{lL}{\Phi C_0}$$

The partition coefficient (Φ) in PEM nanofilm in a feed solution is defined as the ration of the concentration of the analyte in the nanofilm to the concentration of the analyte in the surrounding solution. The partition coefficient can be calculated by taking the ratio of the analyte concentration in the nanofilm to the concentration of the analyte solution in which the nanofilm was initially immersed.

By definition

$$\text{Specific surface} \quad S = \frac{total\ interface\ area}{total\ volume}$$

$$\text{Porosity} \quad \varepsilon = \frac{void\ volume}{total\ volume}$$

$$\text{Available volume fraction} \quad K_{AV} = \frac{available\ volume}{total\ volume}$$

$$\text{Normally } K_{AV} < \varepsilon$$

$$\text{Partition coefficient } \Phi = \frac{K_{AV}}{\varepsilon} \qquad (d: diameter\ of\ pore,\ b: diameter\ of\ solute)$$

$$K_{AV} = \frac{L\pi\left({}^{d}/_{2} - {}^{b}/_{2}\right)^2}{AL}$$

$$\varepsilon = \frac{L\pi\,{}^{d^2}/_{4}}{AL}$$

$$\Phi = \frac{K_{AV}}{\varepsilon} = \frac{{d^2}/{4} + {b^2}/{4} - {bd}/{2}}{{d^2}/{4}} = 1 + \frac{b^2}{d^2} - 2\frac{b}{d} = \left(1 - \frac{b}{d}\right)^2$$

If $\frac{b}{d} \ll 1$, $\Phi \approx 1$ *and* $K_{AV} \approx \varepsilon$

2.3. Results and Discussion

Nanofilms were assembled on bare alumina substrates. PSS, PAA, and PAH were used as film components. The assemblies were characterized by QCM (Figure 7), SEM (Figure 8), ellipsometry (Table 1), and contact angle measurements (Table 1).

From Figure 7, it is clear that the real-time adsorption of PSS/PAH exhibits consistent linear growth due to the strong polyelectrolyte character of PSS. PAA and PAH are both weak polyelectrolytes. Therefore, growth is also influenced by coupling of counter-ion and non-ionic interactions, and is exponential in profile. As observed via SEM (Figure 8), all pores were covered by PEMs after LbL self-assembly, and the different nanofilms possess very different morphology contributed by the different interactions between weak-strong and weak-weak polyelectrolyte pairs.

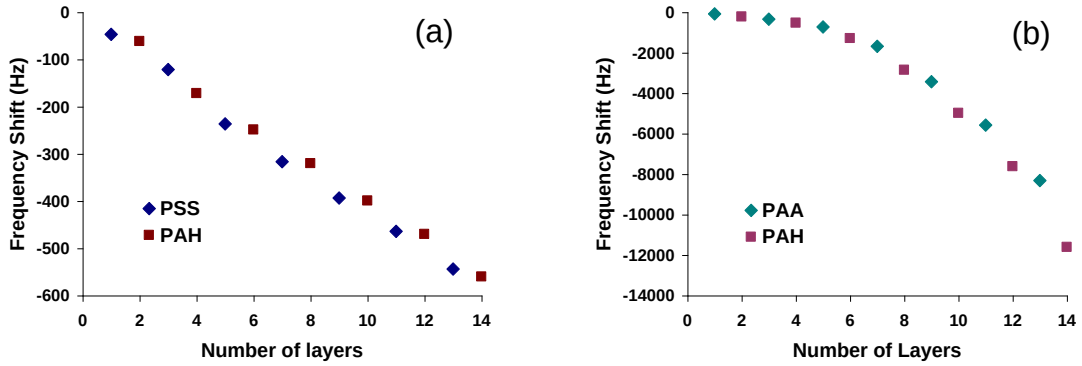

Figure 7. Cumulative frequency shifts (ΔF) vs. layer number between: (a) PSS/PAH; and (b) PAA/PAH alternate adsorption in 0.5 M NaCl aqueous solution.

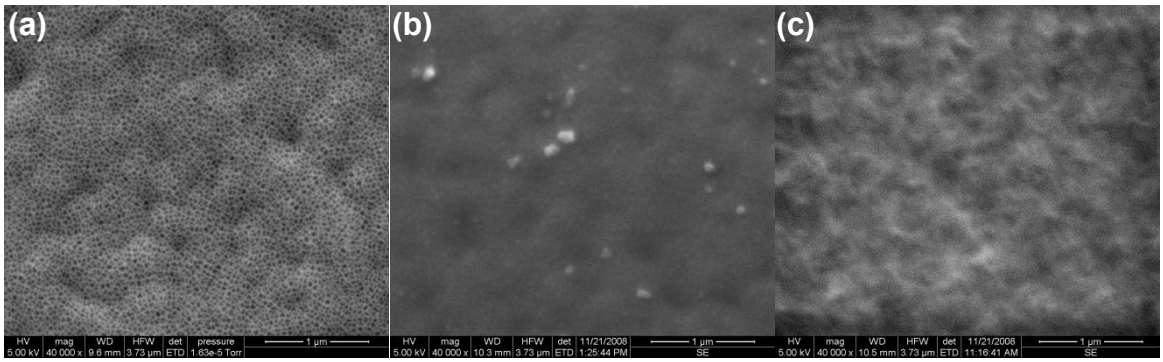

Figure 8. Scanning electron microscope images of nanofilms: (a) bare alumina substrate; (b) $[PSS/PAH]_{6.5}$; and (c) $[PAA/PAH]_{6.5}$. Samples were coated with 5 nm of platinum prior to imaging. All scale bars are 1 μm.

After LbL nanofilm construction, thickness and refractive indices were measured using ellipsometry (in dry condition), and contact angles were also measured with deionized water droplets at the nanofilm-air interface (Table 1). Those measured values (i.e. *L, n, CA*) of nanofilms compared with the values of bare substrate to confirm film construction. Given the level of variability in three measurements, there is no statistical difference between the thickness of 6.5-bilayers and 7-bilayers from each component. However, the thickness of PSS-base and PAA-base films are statistically different each other (t-test, $\alpha = 0.05$).

After verifying film construction on the porous support, diffusion experiments were conducted with each of the nanofilms coatings. Figure 9 shows representative diffusion measurements for nanofilms, and symbols indicate normalized glucose concentration in the permeate ($C_{permeate}/C_{feed}$) at a given time after the feed was spiked with glucose.

Table 1. Thickness (*L*), refractive index (*n*), and static (θ_{static}) contact angle (*CA*) measurements.

Film Composition	*L* (nm)[a]	*n*[b]	*CA* (°)
$[PSS/PAH]_{6.5}$	74.7 (± 4.8)	1.52 (± 0.004)	49 (± 1)
$[PSS/PAH]_{7}$	77.2 (± 6.8)	1.51 (± 0.007)	58 (± 1)
$[PAA/PAH]_{6.5}$	110.8 (± 5.9)	1.44 (± 0.006)	58 (± 1)
$[PAA/PAH]_{7}$	107.7 (± 10.7)	1.46 (± 0.007)	62 (± 1)

( ) indicates an error with 95% confidence interval.

[a] Average thickness (*L*) values measured by ellipsometry in dry condition of nanofilms were used as *dx* in *D* calculations.

[b] Refractive index of the bare alumina substrate was 1.35.

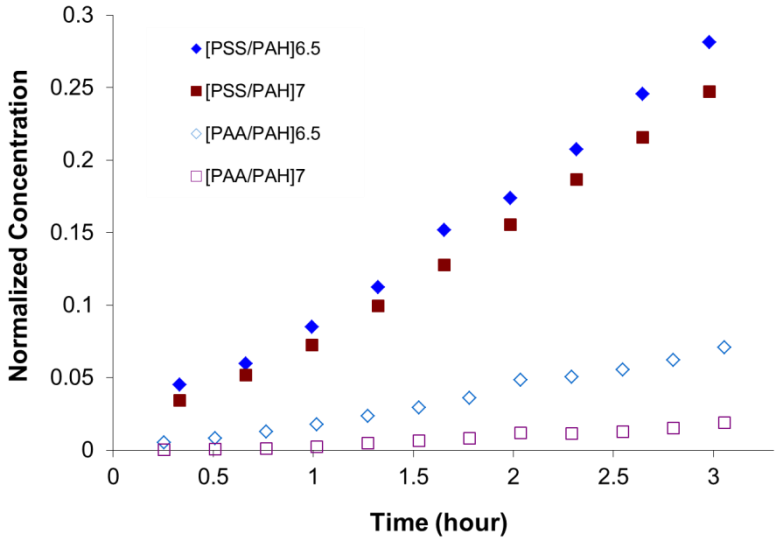

Figure 9. Representative diffusion measurements for nanofilms of different composition.

Nanofilm coatings decreased *D* of glucose up to five orders of magnitude, and [PAA/PAH]-base films generally decreased *D* values of glucose more than [PSS/PAH]-base films did. This is consistent with previous reports, which have shown that one additional PAH terminal layer ($[PSS/PAH]_7$) relative to PSS-terminated film ($[PSS/PAH]_{6.5}$) slightly decreased flux of glucose due to the tighter surface packing of PAH, and the flux of glucose through 5 bilayers of PSS/PAH capped with 1.5 bilayers of PAA/PAH/PAA ($[PSS/PAH]_5[PAA/PAH]PAA$) was 30-fold lower than for $[PSS/PAH]_6PSS$ film.[29, 33] Our *D* values for $[PSS/PAH]_{6.5}$ and $[PSS/PAH]_7$ corresponded with those observations, and *D* values of [PAA/PAH]-base films were

significantly smaller than that of [PSS/PAH]-base films in general (Table 2). Unlike [PAA/PAH]-capped [PSS/PAH] films in the previous work,[29] the *D* value of PAA-terminated nanofilms ($[PAA/PAH]_{6.5}$) was found to be higher than that of PAH-terminated nanofilm ($[PAA/PAH]_7$). *D* values may be correlated with contact angle, but it was found that diffusivity in [PAA/PAH]-base films was independent of contact angle ($\rho(D, CA) = -0.26$).

We found that all of the [PSS/PAH]-based films had an average refractive index of 1.52, while refractive indices of [PAA/PAH]-base films had average values of 1.45. Both of these were found to be significantly different from the refractive index of the bare alumina substrate (1.35). Based previous work, it appears that PAA/PAH films formed under certain pH and ionic strength conditions can undergo morphological transformation to form micro/nanoporous films.[40, 41] It has also been revealed that a pH-induced swelling transition from dense film to nanoporous films results in lower refractive indices in PAA/PAH films (typically changing the refractive index by 0.1-0.2 units).[42, 43]. We tested refractive indices of the nanofilms with different terminal layers to determine whether the [PAA/PAH]-based films exhibited changes in refractive index that would suggest a transition to a nanoporous state (Table 1). We found that the difference in refractive index with different terminal layers is less than 0.02 in all cases. These observations indicate that the terminal layer with different polyelectrolytes does not induce a transition to a nanoporous state.

Table 2. Diffusion coefficients (*D*) of glucose through different nanofilms

Film Composition	*D* (X 10^{-10} cm^2/sec)[a]
$[PSS/PAH]_{6.5}$	4.61 (± 0.293)
$[PSS/PAH]_7$	3.93 (± 0.224)
$[PAA/PAH]_{6.5}$	0.992 (± 0.0514)
$[PAA/PAH]_7$	0.261 (± 0.0457)

( ) indicates an error with 95% confidence interval

[a] *D* value of glucose through bare alumina substrate was 1.15 x 10^{-6} cm^2/sec.

We selected [PSS/PAH]-base films to test the diffusion of different target molecules such as urea (MW 60g/mol) and lactate (MW 90g/mol) in addition to glucose (MW 180g/mol) (Figure 4). Stokes radius of urea, lactate, and glucose is 0.17nm, 0.23nm, 0.36nm, respectively.[44-46] It was observed that nanofilm coatings decreased permeation of target molecules in all cases compared to the bare substrate (Figure 10 shows representative diffusion measurement data for lactate). *D* values of urea were an order of magnitude higher than *D* values of glucose due to their smaller molecular size. *D* values of lactate were between the *D* values of glucose and urea, which also matches expectations based on size. While lactate is an anionic molecule, we did not observe any significant inhibition on diffusivity due to analyte-polymer interaction or coupling with oppositely-charged terminal layers.

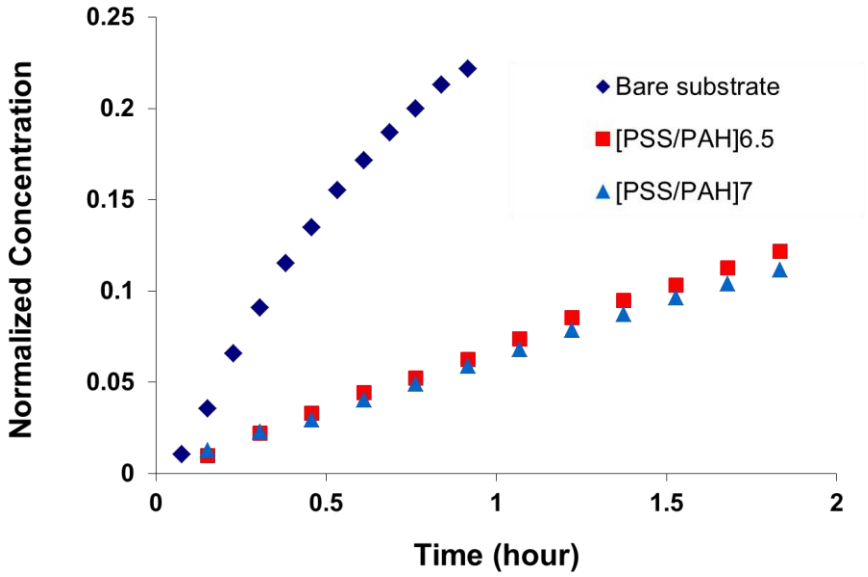

Figure 10. Normalized permeate concentrations of L-lactate versus time during typical diffusion experiments. Nanofilm-coated substrates significantly impeded L-lactate transport, and flux values decreased by a factor of five to six.

After determining *D* values of each glucose, urea, and lactate, we extracted *D* values for each analyte from mixtures of the three analytes (Figure 11). There was no statistical difference between permeation of single-component and multi-component feed solutions (t-test, $\alpha = 0.05$). These results indicate that the nanofilms do not significantly interact with the analytes, and can be utilized for biomolecular sensing of a variety of small molecules with different size and charge.

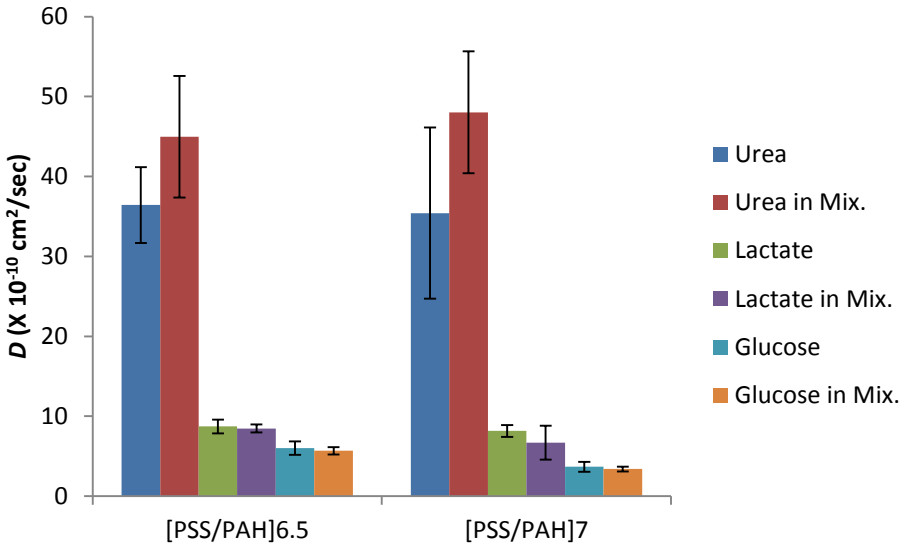

Figure 11. Diffusion coefficients of urea, lactate, and glucose through different nanofilms from individual solution or multicomponent mixture. Error bars represent 95% confidence interval (n=3). *D* values through bare substrate were: D_{urea} = 5.92 X 10^{-6} cm^2/sec; $D_{lactate}$ = 2.20 X 10^{-6} cm^2/sec; $D_{glucose}$ = 1.15 X 10^{-6} cm^2/sec.

2.4. Conclusions

Consecutive film depositions between oppositely-charged polyelectrolytes were characterized using QCM, SEM, ellipsometry, and contact angle measurements. Diffusion coefficients were extracted by regression of flux and concentration gradient data using Fick's law. The specific architectures of the various nanofilms determined the transport properties of target molecules, since permeability of the nanofilms is strongly influenced by the composition of the films and the size of target molecules. Nanofilm coatings near 100nm thickness decreased diffusion coefficients of urea up to

three orders of magnitude, and glucose and lactate up to four orders of magnitude. These results suggest nanofilms can be used as a general strategy for diffusion control, tailored to match the transport requirements of biosensors measuring different target analytes.

3. TUNING OF BIOSENSOR RESPONSE USING MANIPULATION OF NANOFILM COATING PROPERTIES*

3.1. Introduction

Numerous biosensors are currently being developed for monitoring of analytes for both medical and biological purposes.[47-49] However, to be clinically useful, *in vivo* sensors must be able to track changes over the relevant physiological ranges without sacrificing sensitivity and still providing a long working lifetime.[49]

Previous work has shown that the response properties of microspherical enzymatic glucose sensors can be tuned by several different methods. Microspheres with higher porosity allow increased internal oxygen flux, enabling wider glucose concentration range to be sensed.[33] The addition of catalase appears to improve the working lifetime of sensors by consuming the degradative hydrogen peroxide produced by GOx.[50] Catalase also decreases overall glucose sensitivity by producing O_2 in the breakdown of H_2O_2.[50] Manipulation of nanofilm coatings, specifically thickness and/or permeability, is another way to adjust response. Limiting diffusion of glucose into the sensor matrix using PEMs extends the operating range; this diffusion barrier should have the added benefit of reducing exposure of GOx to glucose, which may also prolong sensor lifetime by increasing the amount of time it takes for the enzyme to reach its

---

* Adapted with permission from Collier, B.; Park, J.; McShane, M. *2010 IEEE Sensors* **2010**, 1587-1591.

"turnover number" (the average number of moles of substrate that can be converted before enzyme deactivation). This control over sensor response has, thus far, been achieved by varying the number of layers and the type of materials deposited.[33]

This Section investigated a further aspect of transport properties of PEMs: the role of salt concentration during LbL self-assembly. Charge balance between polyelectrolytes and salt ions is crucial for determining the film growth mechanism and permeability of PEMs.[51-53] In general, higher salt concentrations result in thicker and denser nanofilms due to increased interpenetration of PEMs.[52] We hypothesized that salt concentration in polyelectrolyte deposition solutions would provide another control variable to allow increased tunability of the range and sensitivity of flux-based sensors.

To test this hypothesis, we first deposited nanofilms with various salt concentrations on porous planar substrates and characterized film thickness and glucose diffusion for the coatings prepared with different salt in solution. We then applied the same compositions of nanofilms to our microsphere sensors and measured the response to glucose. The data obtained from the nanofilms on the planar substrate were compared to sensor performance such as sensitivity and range to determine whether decreased glucose diffusion translates into wider range and lower sensitivity.

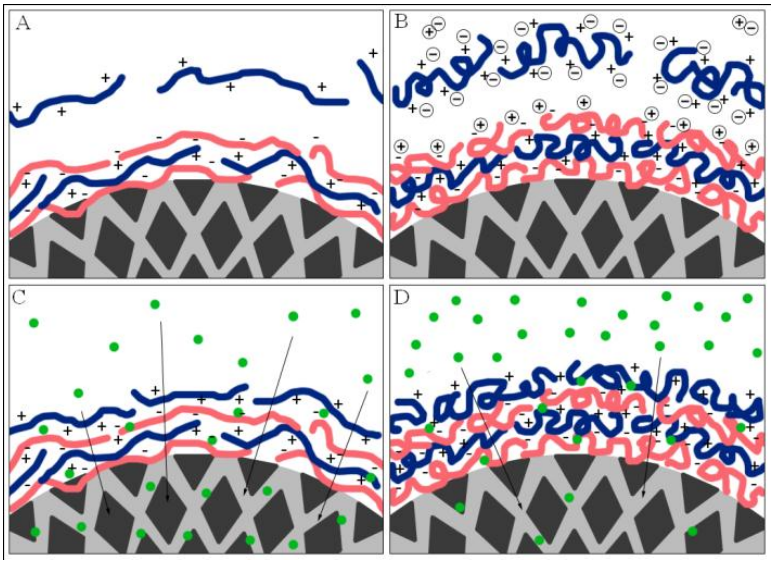

Figure 12. Representation of polyelectrolyte deposition with varying salt concentrations: A) polyelectrolyte deposition without salt present; B) Coiling of polyelectrolyte in the presence of salt during deposition; C) resulting diffusion of glucose (green dots) through the nanofilm; D) the limited glucose diffusion into the sensor matrix. Polyanions and polycations are represented by red and blue lines, respectively. Ions from sodium chloride are shown as circled positive and negative charges.

3.2. Materials and Methods

3.2.1. Materials

Poly(styrene sulfonate) (*PSS*, M_w~70,000) and poly(allylamine hydrochloride) (*PAH*, M_w~70,000) were purchased from Aldrich. Glucose, glucose oxidase, peroxidase, *o*-dianisidine, NaCl, NaOH, HCl, and phosphate buffered saline (PBS) were purchased from Sigma. The porous alumina supports (Anodisc 25, 0.02µm pore diameter) were

purchased from Whatman Ltd. Deionized water (>18.2 MΩcm) was always used for preparation of polyelectrolyte solutions and rinsing. The pH of the polyelectrolyte solutions was adjusted with either HCl or NaOH.

3.2.2. Layer-by-Layer (LbL) self-assembly of nanofilms

Film deposition followed LbL conditions on enzymatic luminescent microsphere sensor. PSS/PAH deposition started with exposure of one side of the alumina support using open-face filter holders (Pall Co.) in 0.02M PSS in different NaCl concentrations (0, 0.01, 0.02, 0.05, 0.1, 0.2, 0.3, 0.4, 0.5 M) adjusted to pH 5 for 10 min. The alumina support was rinsed with deionized water for 1 min before exposure to 0.02M PAH in different NaCl concentrations (0, 0.01, 0.02, 0.05, 0.1, 0.2, 0.3, 0.4, 0.5 M) adjusted to pH 5 for 10 min, followed by another water rinse for 1 min. This process was repeated until 15-bilayers were achieved.

3.2.3. Nanofilm characterization

The properties of nanofilms were characterized by contact angle and thickness measurements. Static (θ_{static}) contact angle (CA) measurements of deionized water droplets at the nanofilm-air interface were measured by goniometer (CAM200, KSV Instruments, Ltd.) at room temperature. Thickness was measured by ellipsometry (EP3-

SE, Nanofilm, Inc.) in a four-zone compensator mode to minimize errors in surface homogeneity.

3.2.4. Diffusion measurements and calculation of diffusivity

Diffusion of glucose through nanofilm coatings were measured using same experimental system described in Section *2.2.4.*. Calculation of glucose diffusivity followed mathematical method described in Section *2.2.5.*.

3.3. Results and Discussion

The thickness of the nanofilms at 0.01M NaCl concentration were slightly decreased relative to no NaCl during the LbL (Figure 13). With continued deposition, the thickness of the nanofilms were significantly increased at each step until the NaCl level at 0.05 M, then stable increasing (but more slowly) at the higher level of NaCl concentrations. This suggests that the nanofilm becomes tighter at the initial low level of NaCl concentration, and grows thicker in the presence of salt. Contact angles of the nanofilms (Figure 14) with different level of LbL salt concentrations also shows that hydrophobicity of its surface is increased with salt concentration until certain level of NaCl (< 0.1 M NaCl).

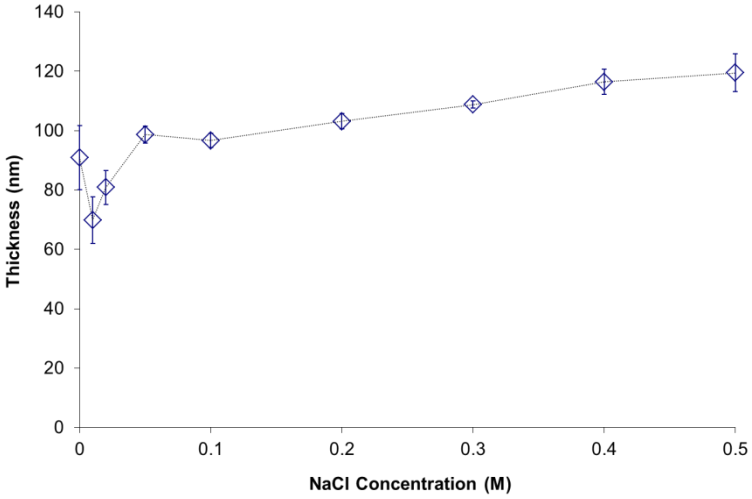

Figure 13. Thickness of $[PSS/PAH]_{15}$ film constructed with different NaCl concentrations (0, 0.01, 0.02, 0.05, 0.1, 0.2, 0.3, 0.4, 0.5 M) during the LbL. Error bars indicate 95% confidence intervals (n=15).

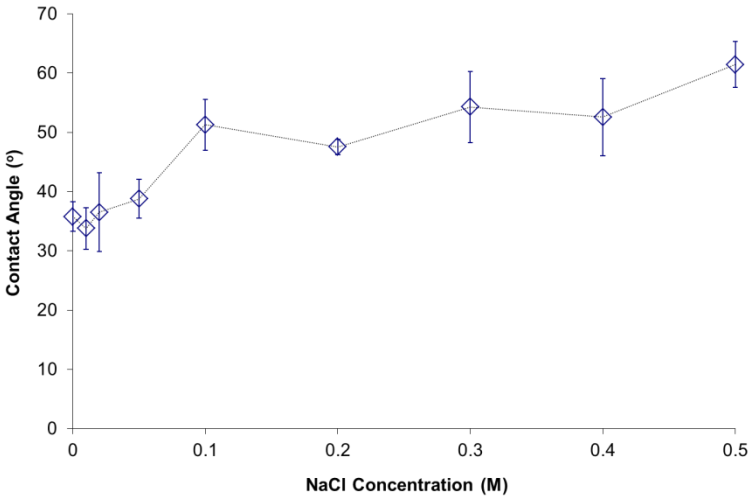

Figure 14. Contact angles of $[PSS/PAH]_{15}$ film constructed with different NaCl concentrations (0, 0.01, 0.02, 0.05, 0.1, 0.2, 0.3, 0.4, 0.5 M) during the LbL deposition. Error bars indicate 95% confidence interval (n=3).

Glucose diffusion through $[PSS/PAH]_{15}$ films constructed with different NaCl concentrations on the planar substrate were observed and compared in terms of sensitivity and range to the behavior of glucose sensors with the same nanofilm coatings. The permeation of glucose through these nanofilms is shown in Figure 15 with the corresponding calculated permeation rates in Figure 16.

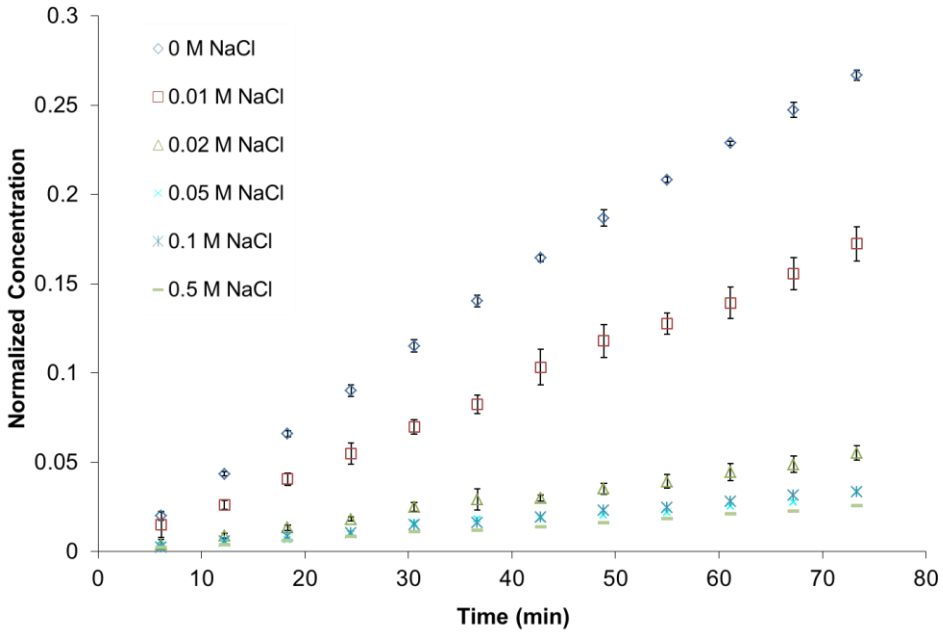

Figure 15. Normalized permeate concentrations of glucose versus time through $[PSS/PAH]_{15}$ films constructed with different NaCl concentrations. Error bars indicate 95% confidence interval (n=3).

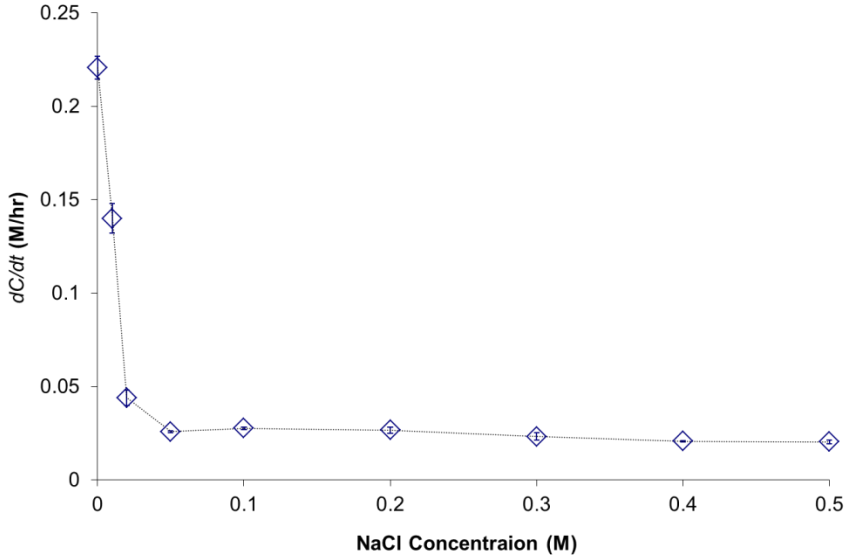

Figure 16. Permeation rate (*dC/dt*) of glucose through $[PSS/PAH]_{15}$ films constructed with different NaCl concentrations. Error bars indicate 95% confidence interval (n=3).

The slopes (*dC/dt*) (Figure 16) show that the nanofilms built from solutions with higher salt concentrations reduce the permeation rate by a factor of ~10 relative to the same nanofilm composition deposited without salt, while the thickness increase from the nanofilm with 0 M NaCl to 0.5 M is less than 32%. This reduced transport of glucose suggests that the nanofilm porosity (also called "tortuosity"[29] in the PEM system) is also lower (tortuosity is higher) when constructed at higher salt concentrations. The corresponding diffusion coefficients (*D*) of glucose through nanofilms with higher salt concentrations are also an order of magnitude lower than the corresponding value without salt (Figure 17), because of large reduction of permeation rate compared to the ~30 nm difference of thickness. However, there is not a significant difference in *D*

values of nanofilms made with solutions of 0.05 and 0.5 M NaCl (α=0.05). Thus, the salt tuning effect is limited in magnitude and is only effective for concentrations up to 0.05 M. This is most likely a result of the concentrations being much larger than polyelectrolyte concentrations (0.02 M), causing polymer coiling to already be near a maximum at 0.02 M NaCl.[4]

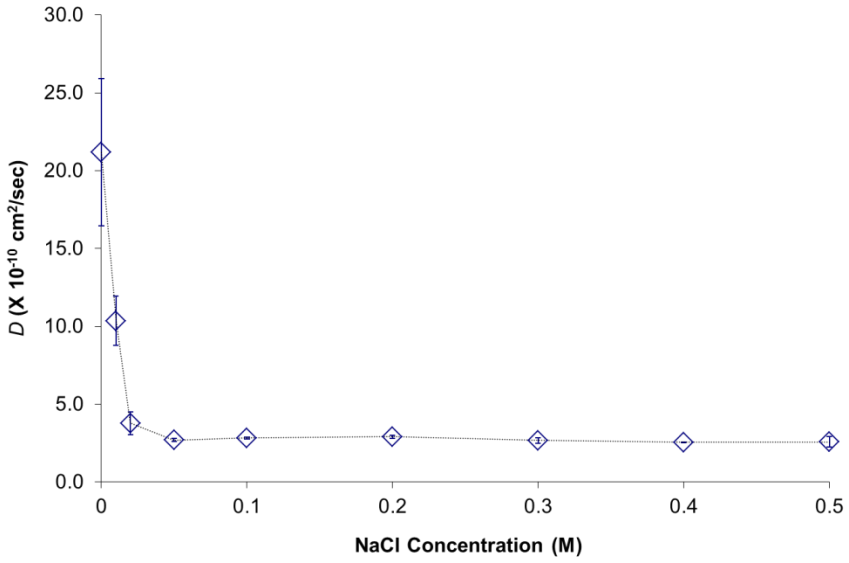

Figure 17. Diffusion coefficients (*D*) of glucose through $[PSS/PAH]_{15}$ films constructed with different NaCl concentrations. Error bars indicate 95% confidence interval (n=3).

The calibration curves obtained from testing the response of sensors to random glucose concentrations are given in Figure 18. As expected, the sensors with nanofilms made in the absence of salt showed a much higher response and smaller range compared

to those sensors with films made in the presence of salt (Table 3). The responses seen from the 0.2 and 0.5 M NaCl films are not significantly different However, correlation coefficient of *dC/dt* and sensitivity in the range of 0 M to 0.5 M is well matched ($\rho(dC/dt, sensitivity) \sim 1$). This finding from microspherical glucose sensor is corresponding with glucose diffusion measurements on the planar substrate.

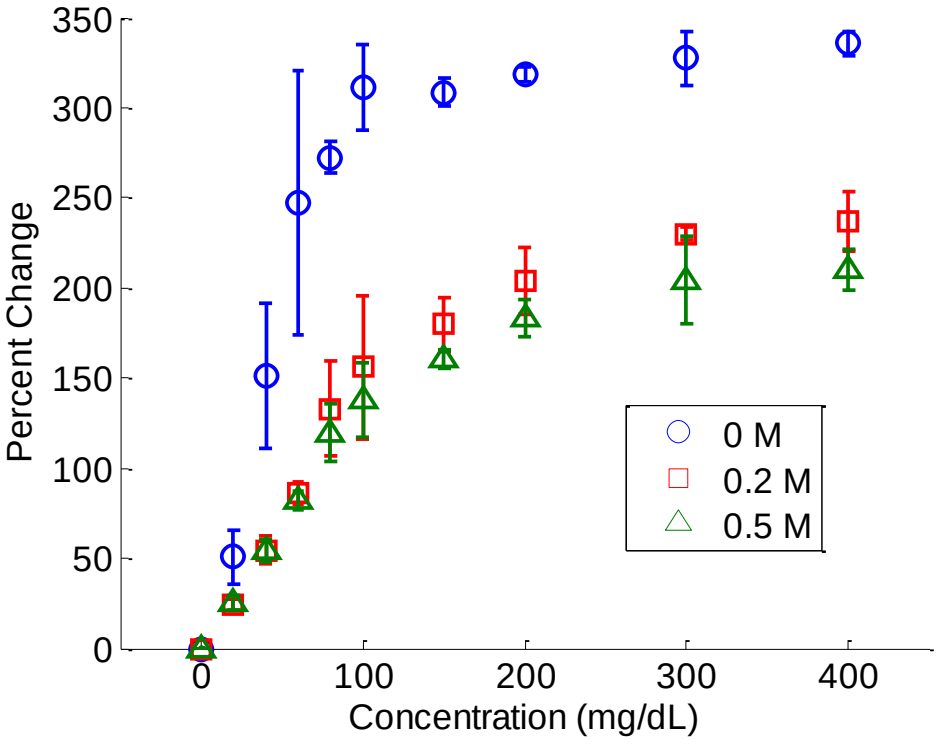

Figure 18. Calibration curves for sensors made with different NaCl concentrations (0, 0.2, and 0.5 M) during deposition of nanofilms comprising $[PSS/PAH]_{15}$. Error bars represent one standard deviation (n = 3). (These data were collected by Brad Collier. See Appendix for experimental description).

Table 3. Permeation rate of nanofilm coatings and responses of microspherical glucose sensor corresponding with various NaCl concentrations during LbL process. ( ) indicates 95% confidence interval (n=3).

NaCl (M)	*dC/dt (M/hour)*	*Senstivity (%/(mg/dL)*	*Range (mg/dL)*
0	0.220 (±0.0006)	4.02 (±0.70)	62.0 (±10.8)
0.2	0.027 (±0.002)	1.40 (±0.39)	148.0 (±64.0)
0.5	0.020 (±0.001)	1.33 (±0.20)	124.3 (±35.9)

3.4. Conclusions

The presence of salt during deposition of diffusion-limiting nanofilms was found to greatly affect glucose permeation and sensor response. The range and sensitivity of the different types of sensors behaved as expected based on the results from nanofilms on the planar substrate, where the decreased glucose diffusion results in decreased sensitivity and increased range. While the added benefit of diffusion-limiting coatings and decreased degradation rate was not demonstrated with the small number of samples in this study, these findings provide insight into another technique to modify flux-based sensor systems without having to re-design using new materials or depositing more layers. Future work will be aimed at determining the nanofilm permeation and sensor response with films created using salt concentrations closer to electrolyte concentrations (0.02 M) to provide increased tunability of sensitivity, range and degradation rate.

4. PROTEIN ADSORPTION ON MULTILAYER COATINGS WITH DIFFUSION-LIMITING NANOFILMS*

4.1. Introduction

Many biosensors require control over both analyte permeability and interaction with the biological environment, such as soluble proteins. Adsorption of proteins on biomaterial surfaces is called fouling, a process that results in "clogging" of pores and, consequently, reduced transport into the material. This is a severe problem for biosensors that rely on analyte flux, because changing permeability will result in altered sensitivity and dynamic range for the sensor response. Therefore, we explored the possibility of combining PEMs with known low glucose permeability with additional outer layers to enhance their resistance to protein adsorption.

PEMs possess inherent nanocomposite structure, which provides for the interesting possibility of designing PEMs with more than one function.[54] PEMs constructed by LbL self-assembly are also extensively used in various biomedical applications such as drug delivery systems,[55-57] and cell engineering.[58-60] However, proteins strongly interact with the polyelectrolyte film regardless of sign of the charges of both the multilayer and the protein,[2] and protein adsorption is the initial event that mediates host response to foreign materials.[3] To further make systems appropriate for *in*

* Adapted with permission from: Park, J.; McShane, M. J. *ACS Appl. Mater. Interfaces* **2010**, *2*, 991-997. Copyright © 2012 American Chemical Society; Park, J.; McShane, M. *2009 IEEE Sensors* **2009**, 1208-1211. Copyright © 2012 IEEE; Park, J.; McShane, M. *2008 IEEE Sensors* **2008**, 562-565. Copyright © 2012 IEEE.

vivo deployment, it is essential to create an interface with the biological system that minimizes the response to the foreign material, such as inflammation and immune system attack, to evade malfunctions of the implants. Masking the implants to avoid protein adsorption enhances biocompatibility and minimizes fouling of surfaces which may alter substrate flux, shifting sensor response profiles.

Poly(ethylene glycol) (PEG) is well known to resist protein adsorption,[61] and can be immobilized on surfaces via hydrogen bonding,[62] covalent attachment,[63] or ionic interaction.[64] Previous work demonstrated PEG-grafted polyelectrolytes with appropriate grafting ratio and length of PEG had strong resistance to nonspecific protein adsorption.[64-68] In this section, poly(L-lysine)-*graft*-PEG (PLL-*g*-PEG) was chosen for surface modification as a surface "comb" of PEG, which has been thoroughly evaluated for toxicity, immunogenicity, pyrogenicity, and biodegradation,[65, 66] This copolymer electrostatically adsorbs to the anionic surface of poly(styrene sulfonate) (PSS) or poly(acrylic acid) (PAA)-terminated PEMs that is compatible with the LbL process without using chemical crosslinking reagents (which is preferred when treating particles with biological activity that must be preserved), and be more stable at broad range of pH than H-bonded films.

As we described in previous sections, determining the transport property of nanofilms with different compositions of materials is critical for *in vivo* applications of biomedical devices. We hypothesized that an outer layer of protein-resistant material could be applied to a pre-fabricated inner layer of glucose transport-limiting material to achieve this dual functionality. To test this hypothesis, we compared different nanofilms

deposited on porous substrates. We applied PEG-modified polyelectrolyte coatings to nanofilms designed for transport control (Figure 19), and the diffusion and protein adsorption of the native transport-controlling films were compared with the PEG-modified versions before and after exposure to albumin solutions and serum.

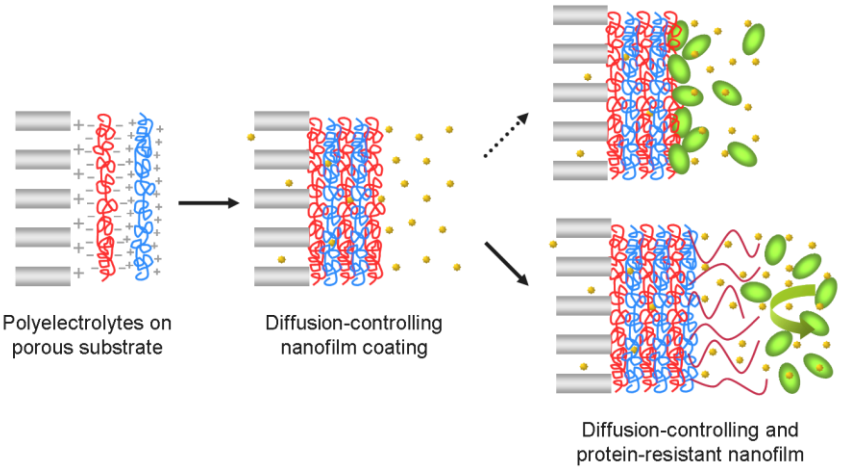

Figure 19. Schematic diagram of dual-functional nanofilms comprising PEMs and PEG-terminated PEMs, exhibiting both diffusion control and resistance to protein adsorption.

4.2. Materials and Methods

4.2.1. Materials

Poly(styrene sulfonate) (*PSS*, M_w=70,000), poly(allylamine hydrochloride) (*PAH*, M_w=70,000), poly(acrylic acid) (*PAA*, M_w=100,000, 35 wt. % in water) and poly(ethyleneimine) (PEI, M_n~60,000, 50 wt. % in water) were purchased from Aldrich.

Glucose, glucose oxidase (GOx), peroxidase, *o*-dianisidine, NaCl, NaOH, HCl, poly(L-lysine) (*PLL*, M_w=12,000~24,000), and bovine serum albumin (BSA) were purchased from Sigma. PLL-*g*[4.5]-PEG (PLL = 20 kDa; PEG = 5 kDa; Lys/PEG graft ratio = 4.5) was purchased from Alamanda Polymers, Inc (Figure 20). Fetal bovine serum (FBS) was purchased from Cascade Biologics. The porous alumina supports (Anodisc 25, 60 μm thick, 0.02 μm pore diameter) were purchased from Whatman Ltd. Deionized water (>18.2 MΩcm) was always used for preparation of polyelectrolyte solutions and rinsing. The pH of the polyelectrolyte solutions was adjusted with either HCl or NaOH.

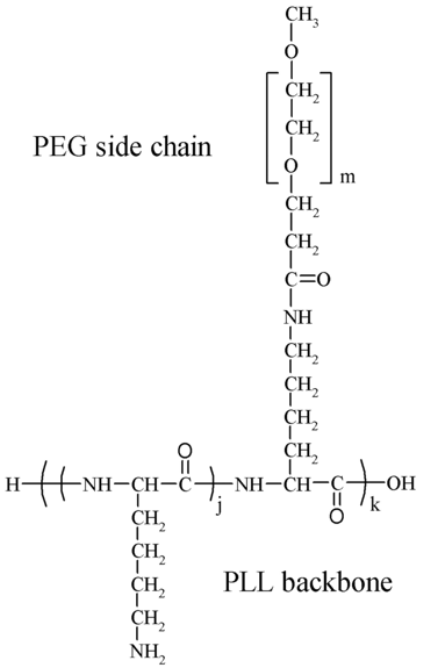

Figure 20. Molecular structure of PLL-g-PEG.

4.2.2. Layer-by-layer (LbL) self-assembly of nanofilms

PSS/PAH deposition started with exposure of one side of the alumina support using open-face filter holder (Pall Co.) in 0.02 M PSS (molarities of polyelectrolytes are given with respect to the repeating unit) in 0.5 M NaCl solution adjusted to pH 2.1 for 5 min. The alumina support was rinsed with deionized water for 1 min before exposure to 0.02 M PSS in 0.5 M NaCl adjusted to pH 2.3 for 5 min, followed by another water rinse for 1 min. PAA/PAH alternative adsorptions involved same deposition and rinse time with 0.02 M PAA (pH 5.5, 0.5 M NaCl) and 0.02 M PAH (pH 5.5, 0.5 M NaCl). We repeated this process until the target number of layers was achieved (more than 5 bilayers are required due to the sufficient surface coverage of PEM).[69] Deposition pH of PAA/PAH followed previous reports, which required conditions of pH higher than 5.0 for PAA adsorption solution, and pH lower than 7.5 for PAH solution.[70-72] These conditions optimize the polyelectrolyte deposited in a highly charged state and colloidal stability, when applied to particle-base biochemical sensor coatings. The PLL and PLL-*g*[4.5]-PEG depositions involved a 5-min exposure in PLL (1mg/mL in phosphate buffered saline (PBS)) and PLL-*g*[4.5]-PEG (1mg/mL in PBS) solutions on top of either PSS or PAH terminal layer. Films were dried with N_2 only after deposition of all layers.

Different combinations of nanofilm assemblies were characterized by scanning electron microscope (SEM, Quanta 600 FE-SEM, FEI Company) and quartz crystal microbalance (QCM, QCM200, Stanford Research Systems, Inc.). Static (θ_{static}) contact angle (CA) measurements of deionized water droplets at the nanofilm-air interface were

measured at room temperature using goniometer (CAM200, KSV Instruments, Ltd.) with measuring a 3 μL sessile drop of water at 30 sec after deposition onto the nanofilm surfaces. Thickness and refractive index was measured by ellipsometry (EP3-SE, Nanofilm, Inc.) with an incident angle of 54° and a wavelength of 532 nm in a four-zone compensator mode to minimize errors in surface homogeneity.

4.2.3. Measurements of Protein Adsorption

AT-cut quartz crystals with a fundamental resonance frequency of 5 MHz were cleaned by immersion into a 1:1:5 solution of H_2O_2 (30% w/w), NH_4OH (25% w/w), and deionized water heated to a temperature of about 75 °C for 5 min followed by immediately rinse with deionized water and drying with N_2. The gold surface of the quartz crystal was immersed for 10 min in 0.02 M PEI solution containing 0.5 M NaCl to create a positively charged substrate surface. Then LbL deposition of nanofilms was conducted following the same procedure as Section *4.4.2.*. The quartz crystal was rinsed by deionized water for 1 min before loading to the QCM liquid flow cell. Flow through the QCM cell coated with nanofilm was present during the all frequency measurements including stabilization, protein adsorption, and rinsing steps. Either BSA (1 mg/mL in PBS) or FBS (used as purchased) solution was introduced into the flow system for one hour after rinsing and stabilizing the QCM frequency, and frequency shifts were continuously monitored after rinsing with PBS. The mass was determined from the measured frequency using Sauerbrey's equation.[73]

4.2.4. Diffusion measurements and calculation of diffusivity

Diffusion of glucose through nanofilm coatings before and after BSA and FBS exposures were measured using same experimental system described in Section *2.2.4.*. Calculation of glucose diffusivity followed mathematical method described in Section *2.2.5.*.

4.3. Results and Discussion

Nanofilms were assembled on bare alumina substrates. PSS (strong polyanion), PAA (weak polyanion), PAH (weak polycation), PLL (weak polycation), and PLL-*g*-PEG were used as film components. The assemblies were characterized by SEM (Figure 21), ellipsometry (Figure 23, Table 5), contact angle measurements (Table 4), and QCM (Figure 7). As observed via SEM, all pores were covered by PEMs after LbL self-assembly, and the different nanofilms possess very different morphology contributed by the different interactions between weak-strong and weak-weak polyelectrolyte pairs as well as the grafted PEG side chains (Figure 21).

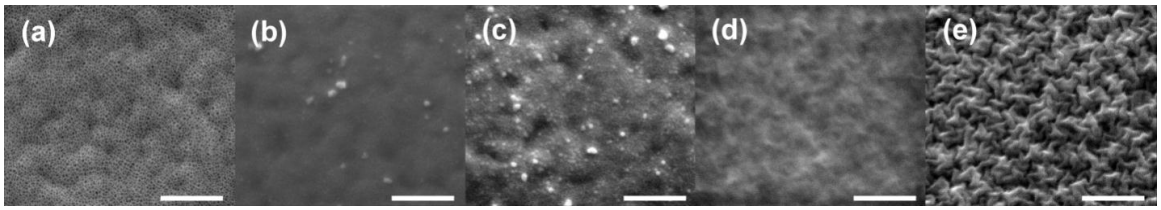

Figure 21. Scanning electron microscope images of nanofilms: (a) bare alumina substrate; (b) [PSS/PAH]6PSS; (c) [PSS/PAH]6PSS/PLL-g-PEG; (d) [PAA/PAH]6PAA; and (e) [PAA/PAH]6PAA/PLL-g-PEG. Samples were coated with 5 nm of platinum prior to imaging. All scale bars are 1 μm.

We directly determined protein uptake on the different films ($[PSS/PAH]_6PSS$, $[PSS/PAH]_6PSS/PAH$, $[PSS/PAH]_6PSS/PLL$, and $[PSS/PAH]_6PSS/PLL$-*g*-PEG) via QCM (Figure 22a). Real-time protein adsorption after BSA introduction on the different nanofilms indicated that almost 90 % of adsorption takes place within 5 min. QCM measurements of mass changes indicated a substantial improvement in adsorption resistance with the addition of the final PLL-*g*-PEG layer. PLL-*g*-PEG coatings were the most resistant to albumin adsorption of the films considered, and PEG decreases the albumin mass to below the detection limit of the technique (< 45 ng/cm^2) compared to unmodified PSS (736 ± 52 ng/cm^2), PAH (567 ± 18 ng/cm^2), and PLL (658 ± 39 ng/cm^2) (Figure 22b). This is consistent with previous reports on PEGylation for similar materials.[64, 65, 74]

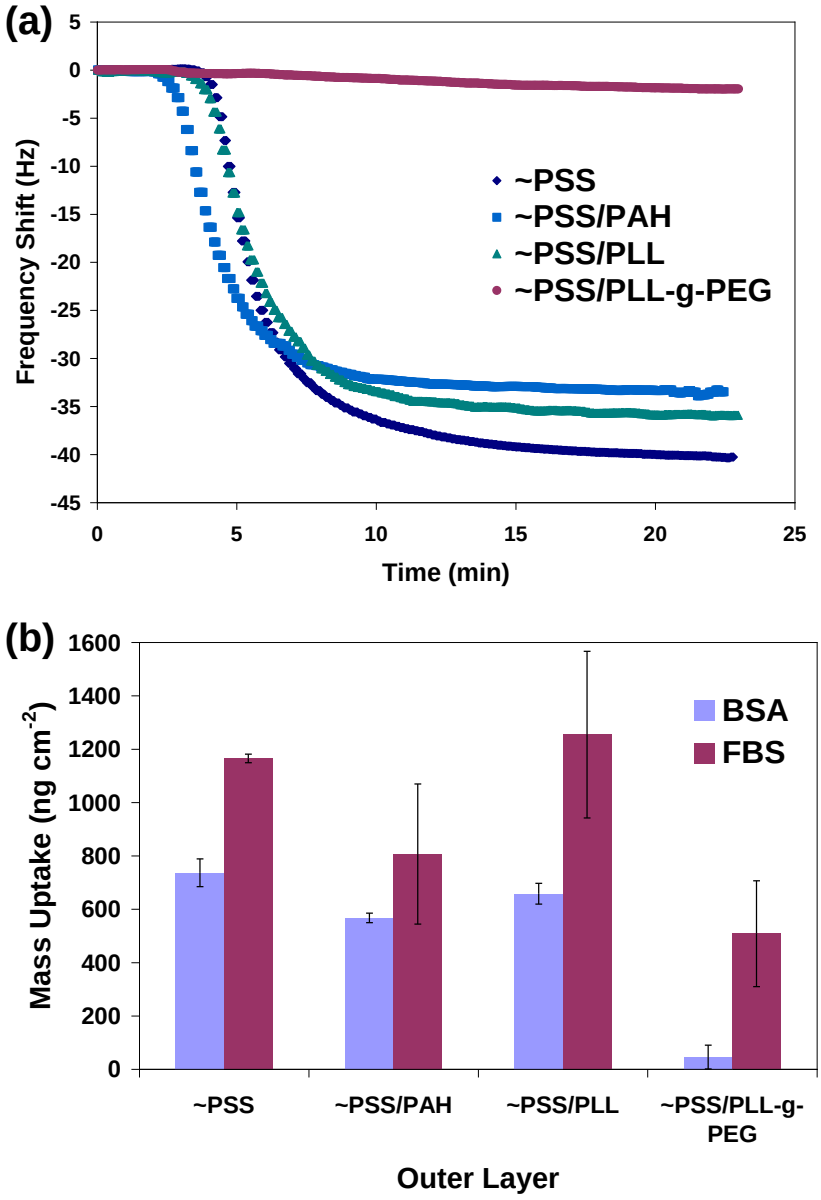

Figure 22. (a) Real-time QCM frequency shifts after BSA introduction on the different nanofilms; (b) Mass uptake to nanofilms with different outermost layers on top of the base-$[PSS/PAH]_6$ multilayer, measured by QCM after exposure of BSA and FBS. PLL-*g*-PEG outer layer improved resistance to BSA (*p-value* < 0.005), but less dramatic improvement in serum (*p-value* < 0.1).

Interestingly, the quantity of protein adsorption on the unmodified films was not directly related with charge of the surface layer and only weakly correlated with the contact angle of the films (correlation coefficient, ρ(CA, mass uptake) = 0.77). In all nanofilms, an adsorbed mass increases after FBS exposure were higher than those due to BSA, indicating serum proteins and potentially other molecules in the serum attach to or penetrate into nanofilms.[75, 76] These components may also change the environment (e.g. viscosity, charge density) around PEMs on the quartz crystal electrode. Surprisingly, investigations of protein adsorptions on [PAA/PAH]-base films with different final layers revealed unstable signals from QCM after protein solution was introduced even for PEG-terminated films, suggesting a susceptible nature of the underlying PEMs. It is noteworthy that the susceptibility of weak-weak polyelectrolyte pairs to environmental changes has been previously observed.[77-79]

Table 4. Static (θ_{static}) contact angle (*CA*) measurements of deionized water droplets at the nanofilm-air interface.

Film Composition	*CA* (°C)
$[PSS/PAH]_6PSS$	49 ± 1
$[PSS/PAH]_6PSS/PAH$	58 ± 1
$[PSS/PAH]_6PSS/PLL$	42 ± 1
$[PSS/PAH]_6PSS/PLL$-g-PEG	28 ± 1
$[PAA/PAH]_6PAA$	58 ± 1
$[PAA/PAH]_6PAA/PAH$	62 ± 1
$[PAA/PAH]_6PAA/PLL$	63 ± 1
$[PAA/PAH]_6PAA/PLL$-g-PEG	39 ± 3

The thickness of different multilayers on the porous alumina substrate was measured by ellipsometry (Figure 23). It was observed that the thickness before and after serum exposure was not statistically different in any films, despite the apparently large changes observed via QCM; this was expected, since the native nanofilms were ~100 nm, and an added layer of proteins adsorbed onto the nanofilm surface would add only 5-10 nm. However, the thickness of [PSS/PAH]-base films (strong-weak PE interaction) and [PAA/PAH]-base films (weak-weak PE interaction) were different (*p-value* < 0.01) regardless of serum adsorption. These ellipsometry results provide evidence that weak-weak PEMs are thicker and highly interpenetrated structure than strong-weak PEMs, and this is compatible with previous reports.[77, 78] It is also noteworthy that none of the coatings exhibited a decrease in thickness due to protein exposure, suggesting that the environment of the protein-containing solutions does not result in disintegration of the nanofilms.

As described in Section 2, *D* values of [PAA/PAH]-base films were significantly smaller than that of [PSS/PAH]-base films in general (Table 5). We also found that PEGylated surfaces maintained their diffusion property in the same order of magnitude as nanofilms with the same underlying composition. The refractive indices of $[PAA/PAH]_6PAA$ films did not exhibit any significant change upon addition of capping layers of PLL or PLL-*g*-PEG. These observations confirmed again with results from Section 2 that surface modification with different polyelectrolytes does not induce a transition to a nanoporous state. This agrees with expectations, as the pH of the PLL and PLL-*g*-PEG solution used for adsorption was neutral.

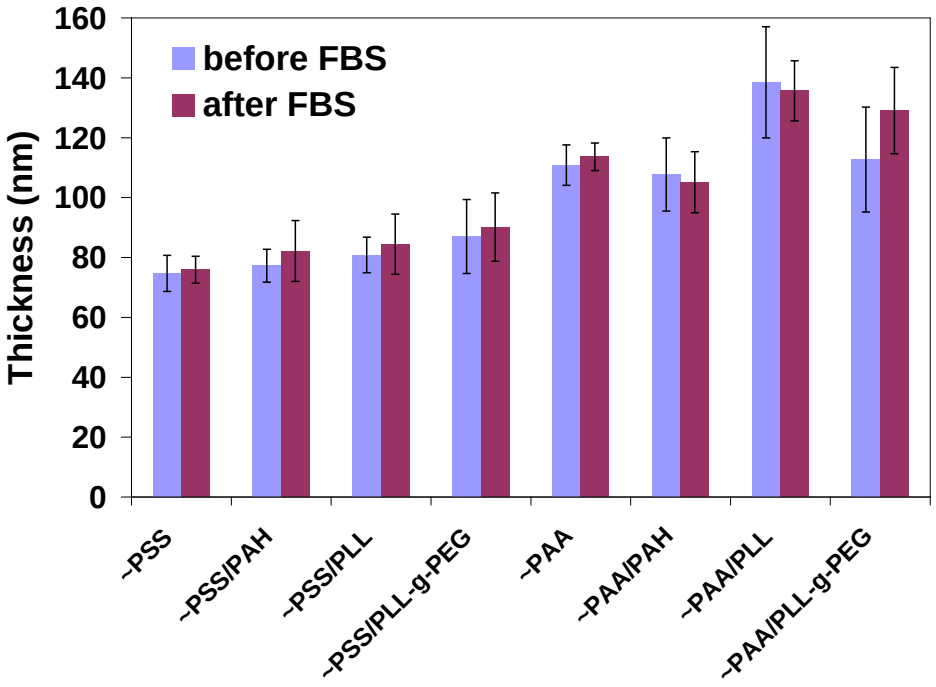

Figure 23. Nanofilm thickness with different outermost layers before and after immersing in FBS, as measured by ellipsometry. All films were measured in dry state. The first-half of the x-axis indicates final layer set on top of $[PSS/PAH]_6$, and the second-half indicates final layer set on top of $[PAA/PAH]_6$ on the alumina substrate. Error bars indicate one standard deviation from fifteen measurements.

On the basis of previous work and above results, we appreciate the fact that the structure of PAA/PAH multilayers can be affected by small change of environment. Our main concern is the susceptibility to changes in physiological conditions for *in vivo* applications, and particularly whether this susceptibility is altered by the presence of a "capping" layer of PLL-*g*-PEG, which theoretically would protect the underlying layers from interactions with large proteins. Our primary focus is on how the diffusivity of these weak-weak polyelectrolyte pairs can be affected before and after protein and serum

exposure relative to strong-weak pairs. We observed that the underlying films played a more important role in the response to proteins, whether it was modified with protein-resistance surface or not.

Table 5. Thickness (*L*), refractive index (*n*) of nanofilms, and diffusion coefficients (*D*) of glucose through nanofilms.

Nanofilm Composition	*L* (nm)[a]	*n* [b]	$D_{glucose}$ (X 10^{-10} cm^2/sec)[c]
$[PSS/PAH]_6PSS$	74.7 ± 6.0	1.52 ± 0.004	4.61 ± 0.37
$[PSS/PAH]_6PSS/PAH$	77.2 ± 5.5	1.51 ± 0.008	3.93 ± 0.28
$[PSS/PAH]_6PSS/PLL$	80.8 ± 5.9	1.51 ± 0.005	4.03 ± 0.22
$[PSS/PAH]_6PSS/PLL$-g-PEG	87.0 ± 12.3	1.51 ± 0.007	2.54 ± 0.22
$[PAA/PAH]_6PAA$	110.8 ± 6.8	1.44 ± 0.006	0.99 ± 0.07
$[PAA/PAH]_6PAA/PAH$	107.7 ± 12.2	1.46 ± 0.007	0.26 ± 0.06
$[PAA/PAH]_6PAA/PLL$	138.5 ± 18.5	1.47 ± 0.019	1.01 ± 0.06
$[PAA/PAH]_6PAA/PLL$-g-PEG	112.7 ± 17.5	1.45 ± 0.008	0.22 ± 0.02

a. Average thickness (*d*) values measured by ellipsometry were used as *dx* in *D* calculations, and feed gradient *dC/dx* assumed constant for linear permeate concentration increase.
b. Refractive index of the bare alumina substrate was 1.35.
c. *D* value of glucose through bare alumina substrate was 1.15 x 10^{-6} cm^2/sec.

After determining *D* values of glucose through various nanofilms, we investigated how transport properties of nanofilms are affected by protein adsorption on the films as might be experienced by implanted devices (Figure 24). Overall, *D* values of [PSS/PAH]-base films after protein and serum exposure had excellent correspondence

with original *D* values of native films, particularly for PLL-terminated and PLL-*g*-PEG-terminated nanofilms. No statistical difference of *D* values was observed in between after protein exposure and serum exposure in the same composition of the films, except $[PAA/PAH]_6PAA/PAH$ and $[PAA/PAH]_6PAA/PLL$ films; these materials did not permeate glucose after serum exposure (glucose concentration below the detection limit of colorimetric assay via plate reader). Glucose diffusivity in $[PSS/PAH]_6PSS/PLL$ and $[PSS/PAH]_6PSS/PLL$-*g*-PEG films was minimally affected after protein adsorption (+5.7 %, +11.3 % respectively) and serum exposure (+12.2 %, -2.2 % respectively). Even though the diffusivity of $[PSS/PAH]_6PSS/PLL$ was not strongly influenced by protein exposure, it still has some protein adsorption (Figure 22), which might alter flux and/or mediate host responses for *in vivo* applications. However, strong interactions with protein solutions were observed in all [PAA/PAH]-base films, with more dramatic changes after serum exposure.

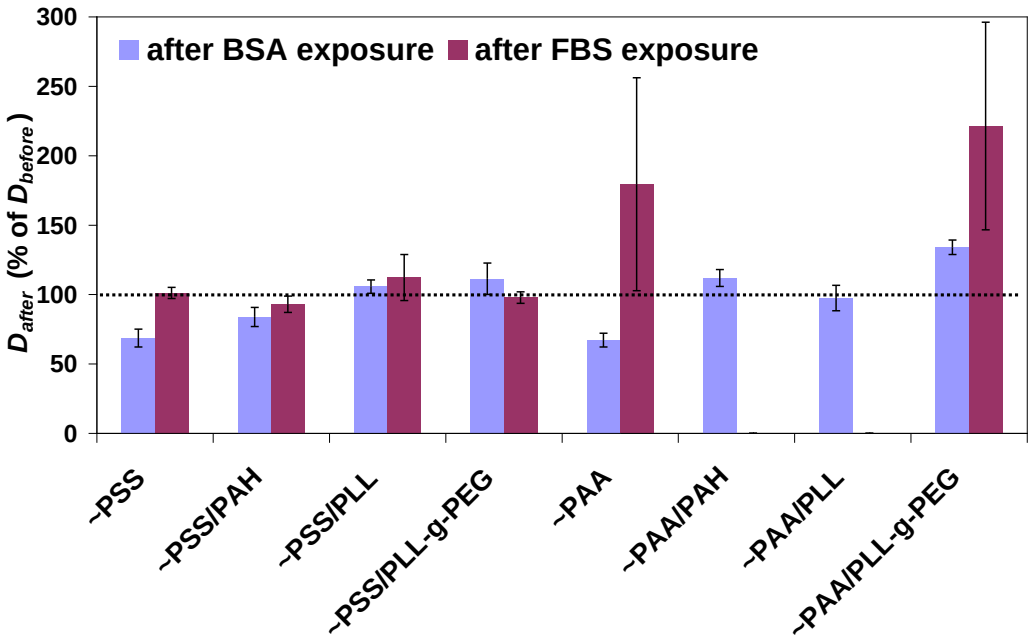

Figure 24. Change in glucose diffusivity in nanofilms after BSA and FBS exposure. The first-half of the x-axis indicates final layer set on top of $[PSS/PAH]_6$, and the second-half indicates final layer set on top of $[PAA/PAH]_6$. Each bar indicates relative % of mean *D* value after BSA and FBS exposures from *D* values of native nanofilm (100 %, dashed line) before protein and serum exposures. Error bars represent the 95% confidence interval (n=3).

We also measured glucose diffusivity with $[PSS/PAH]_6$PSS/PLL-g-PEG, $[PAA/PAH]_6$PAA, and $[PAA/PAH]_6$PAA/PLL-g-PEG after exposure to serum for 24 hours (Figure 25). $[PSS/PAH]_6$PSS/PLL-g-PEG still maintains glucose diffusivity as we expected, while weak-weak PEMs are not stable. SEM images after exposure to serum also support $[PAA/PAH]_6$PAA and $[PAA/PAH]_6$PAA/PLL-g-PEG films were strongly influenced by serum exposure compare to the native films (Figure 26).

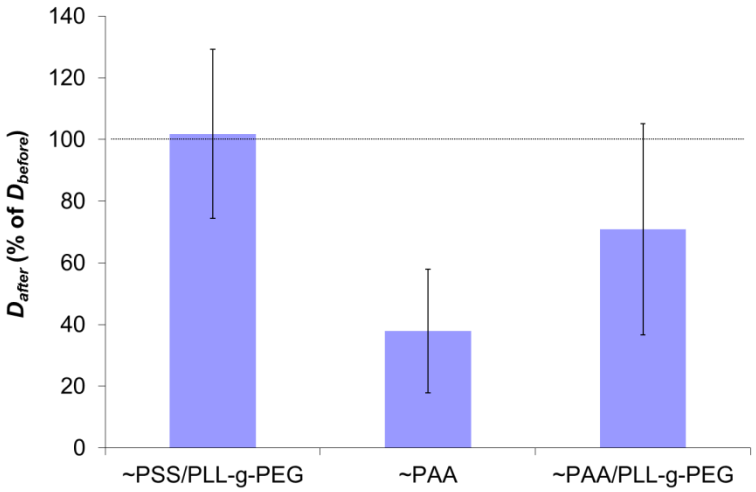

Figure 25. Change in glucose diffusivity in nanofilms after 24 hour exposure to FBS. Error bars represent the 95% confidence interval (n=3).

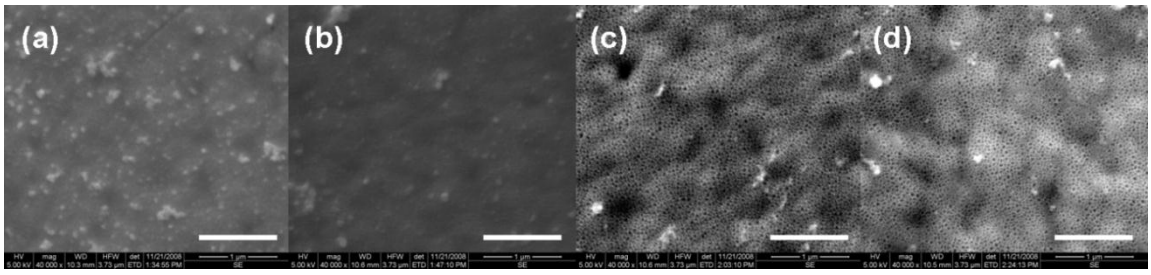

Figure 26. Scanning electron microscope images of nanofilms after exposure to FBS: (a) $[PSS/PAH]_6PSS$; (b) $[PSS/PAH]_6PSS/PLL\text{-}g\text{-}PEG$; (c) $[PAA/PAH]_6PAA$; and (d) $[PAA/PAH]_6PAA/PLL\text{-}g\text{-}PEG$. Samples were coated with 5 nm of platinum prior to imaging. All scale bars are 1 μm.

Based on the protein adsorption experiment, we conclude [PAA/PAH]-base films were strongly affected by both protein and serum exposure even in the PLL-*g*-PEG finalized film, and the susceptible nature of these weak-weak PEMs caused large variation in *D* values of glucose. We also note that chemical crosslinking is an option to improve the stability of the PAA/PAH films, which our findings suggest is a necessary treatment if these specific materials are desired for use.

4.4. Conclusions

Our findings suggest that careful analysis of materials is required to reveal potential problems for *in vivo* biosensor coating applications; it is not sufficient to combine two multilayers with desirable properties and assume they will combine independently to provide the dual function. Along with the desired diffusion control, the susceptibility of underlying multilayers to environmental influence must be considered. In the case of our study on glucose diffusion, it was revealed that weak-weak PEMs should not be used to control transport due to their irregular behavior under physiological conditions, even though they offer superior diffusion resistance.

Application of a terminal layer of protein-resistant material does not substantially affect total film permeability—due to the much lower relative diffusivity, this characteristic is determined by the underlying films. Despite the lower permeability to glucose compared to strong-weak films, weak-weak films exhibited large variation in

permeability after protein exposure, even when PEG surface coatings were applied. In contrast, strong-weak pairs were more robust and maintained stable diffusion control when exposed to proteins. Thus, multilayers of strong-weak pairs should be used to achieve and maintain the desired flux balance, which may require deposition of thicker layers to obtain lower permeability. It is also possible that more complex combinations of strong-weak with intervening weak-weak domains could be considered. This will be one aspect of our future work on these interesting and useful nanofilm systems.

5. BIOLOGICAL POLYELECTROLYTE MULTILAYERS

5.1. Introduction

The need to understand a biointerface with nanometer-scale control over its properties and functions has become more pronounced in recent years. Biomaterial surfaces have considerable importance to biotechnology and biomedical applications as they influence molecular cell and tissue events, including cell adhesion, protein adsorption, and host response to foreign materials.[80] One of the crucial properties in biological systems that depends strongly on this biomaterial interaction is the transport behavior of membranes at the material interfaces. For example, implantable chemical sensing and drug release systems require diffusion-limiting coatings to act as transport barriers for specific molecules.[32, 33, 81-83] However, the interfacial behaviors of these coatings can vary widely as a result of their interactions with the surrounding biology.

Considerable efforts have been devoted towards the functionalization of the biomaterial surfaces commonly used in biomedical applications to provide them with new functional biological properties and to render them more biomimetic, the self-organization of natural matrices.[84, 85] The possibilities for using a wide range of polyelectrolytes combined with the advantages offered by PEM coatings, such as spatial confinement and localized delivery, as well as protective effects on exposure to physiological media and external stresses, considerably enrich the biological applications for PEM films.[84] These materials have been widely used as biocompatible

and biodegradable materials in biomedical applications including drug delivery, biosensors, and tissue engineering.[84, 85]

Transport properties of synthetic polyelectrolyte multilayers have been studied in previous sections. In this section, native and crosslinked diffusion-limiting nanofilms composed of various combinations of natural and/or synthetic biopolyelectrolytes, such as alginate, dextran sulfate, heparin, poly(L-glutamic acid), poly(L-lysine), and chitosan, are explored.

5.2. Materials and Methods

5.2.1. Materials

Glucose, glucose oxidase, peroxidase, *o*-dianisidine, NaCl, NaOH, HCl, poly-L-lysine hydrobromide (*PLL,* M_w=15,000-30,000), and alginic acid sodium salt from brown algae (*Alg*, low viscosity) were purchased from Sigma. Heparin sodium salt (*Hep*), dextran sulfate sodium salt (*DS*, M_w>500,000), and *N*-(3-Dimethylaminopropyl)-*N*′-ethylcarbodiimide hydrochloride (EDC) were purchase from Sigma-Aldrich. Poly-L glutamic acid sodium salt (*PGA,* M_v=15,000-50,000) and chitosan (*Chi,* M_w ~ 50,000) were purchased from Aldrich. *N*-hydroxysuccinimide (NHS) was obtained from Toronto Research Chemicals Inc. The porous alumina supports (Anodisc 25, 60 μm thick, 0.02 μm pore diameter) were purchased from Whatman Ltd. Deionized water

(>18.2 MΩcm) was always used for preparation of polyelectrolyte solutions and rinsing. The pH of the polyelectrolyte solutions was adjusted with either HCl or NaOH.

5.2.2. Layer-by-layer self-assembly of biopolyelectrolytes

Electrostatic interactions between polyanions (alginate, dextran sulfate, heparin, and poly(L-glutamic acid)) and polycations (poly(L-lysine) and chitosan) were repeated until the desired number of layers was achieved. PLL-based LbL depositions started with exposure of one side of the alumina support using open-face filter holder (Pall Co.) in 1 mg/mL solution of each polyanion in phosphate buffered saline (PBS, pH 7.4) for 10 min. The alumina support was rinsed with PBS (pH 7.4) for 1 min before exposure to 1 mg/mL PLL in PBS for 10 min, followed by another PBS rinse for 1 min. Chitosan-based LbL adsorptions involved 10 min deposition with 1mg/mL of each polyanion in 0.15 M NaCl solutions adjusted to pH 5.5 and 1 mg/mL chitosan in 0.15 M NaCl solution adjusted to pH 5.5. All chitosan-based multilayers were rinsed with 0.15 M NaCl during LbL self-assembly. This process for all combinations (Alg/PLL, DS/PLL, Hep/PLL, PGA/PLL, Alg/Chi, DS/Chi, Hep/Chi, and PGA/Chi) repeated until the target number of layers (i.e. 6.5 and 7 bilayers) was achieved. Films were dried with N_2 only after deposition of all layers.

5.2.3. Nanofilm characterization

As described in Section *2.2.3.*, different combinations of nanofilm assemblies were characterized by quartz crystal microbalance (QCM, QCM200, Stanford Research Systems, Inc.), static contact angle (θ_{static}, CA) measurements, and ellipsometry (EP3-SE, Nanofilm, Inc.). All measurements were performed before and after crosslinking of BPEMs.

5.2.4. Quartz Crystal Microbalance Measurements for alternative adsorption of BPEMs

AT-cut quartz crystals with a fundamental resonance frequency of 5 MHz were cleaned by immersion into a 1:1:5 solution of H_2O_2 (30% w/w), NH_4OH (25% w/w), and deionized water heated to a temperature of about 75 °C for 5 min followed by an immediate rinse with deionized water and drying with N_2. The quartz crystal was loaded into the QCM liquid flow cell. Each solution of biopolyelectrolytes described above was alternatively introduced into the flow system after rinsing and stabilizing the QCM frequency until the desired number of layers was reached. Frequency shifts were measured before, during, and after exposure to the biopolyelectrolyte solutions, and measurements were performed under continuous flow at 50 µl/min. As described previously, the mass was determined from the measured frequency using Sauerbrey's equation.[73]

5.2.5. Crosslinkng of BPEMs

Crosslinking was conducted on the pre-deposited films which contained –COOH in the polyanions and $–NH_2$ in the polycations (i.e. Alg/PLL, Hep/PLL, PGA/PLL, Alg/Chi, Hep/Chi, and PGA/Chi). Crosslinking reactions were performed on porous alumina supports and on silicon substrates (for ATR-FTIR measurements). EDC (200 mM) and NHS (50 mM) were dissolved in 0.15 M NaCl solution adjusted to pH 5.5. The substrate with pre-deposited nanofilms was immersed in the EDC/NHS solution for 12 h at 4 °C as previously reported.[86]

5.2.6. Diffusion measurements and calculation of diffusivity

Diffusion of glucose through BPEMs before and after crosslinking were measured using the same experimental system described in Section *2.2.4.*. Calculation of glucose diffusivity followed the mathematical method described in Section *2.2.5.*.

5.3. Results and Discussion

Quartz crystal resonator measurements revealed that all of the combinations yielded nanofilms with mass increasing with growing number of layers (Figure 27). According to previous reports, this type of growth was mostly observed when a high

degree of polyelectrolyte inter-diffusion was found.[87, 88] It was observed that Alg/PLL, DS/PLL, and PGA/PLL exhibited highly exponential film growth with 14 layer deposition.

Thickness and hydrophobicity of multilayer films are key factors of the transport properties of multilayer films. Thickness is the essential parameter for calculating the diffusion coefficient and surface wettability affects permeability of the film to target species.[89, 90] These two parameters were measured for each material combination in an attempt to identify characteristics that correlate with small molecule (i.e. glucose) diffusion. Average thickness values of all PLL-based multilayers are in the range of 103 to 140 nm, while those of Chi-based films vary with their compositions from 41 to 126 nm (Table 6).

Furthermore Alg/Chi and PGA/Chi films are especially thinner than the others because of multilayer structures with differences in chain lengths and stiffness of polyelectrolytes. Maurstad *et al.* have reported that compression and rearrangements occur in larger polyelectrolytes during the adsorption process.[91] A previous report also showed the thickness of $[Alg/Chi]_{6.5}$ to be ~ 45 nm as measured by QCM, which agrees with our ellipsometric measurement (41± 5.0 nm).[92]

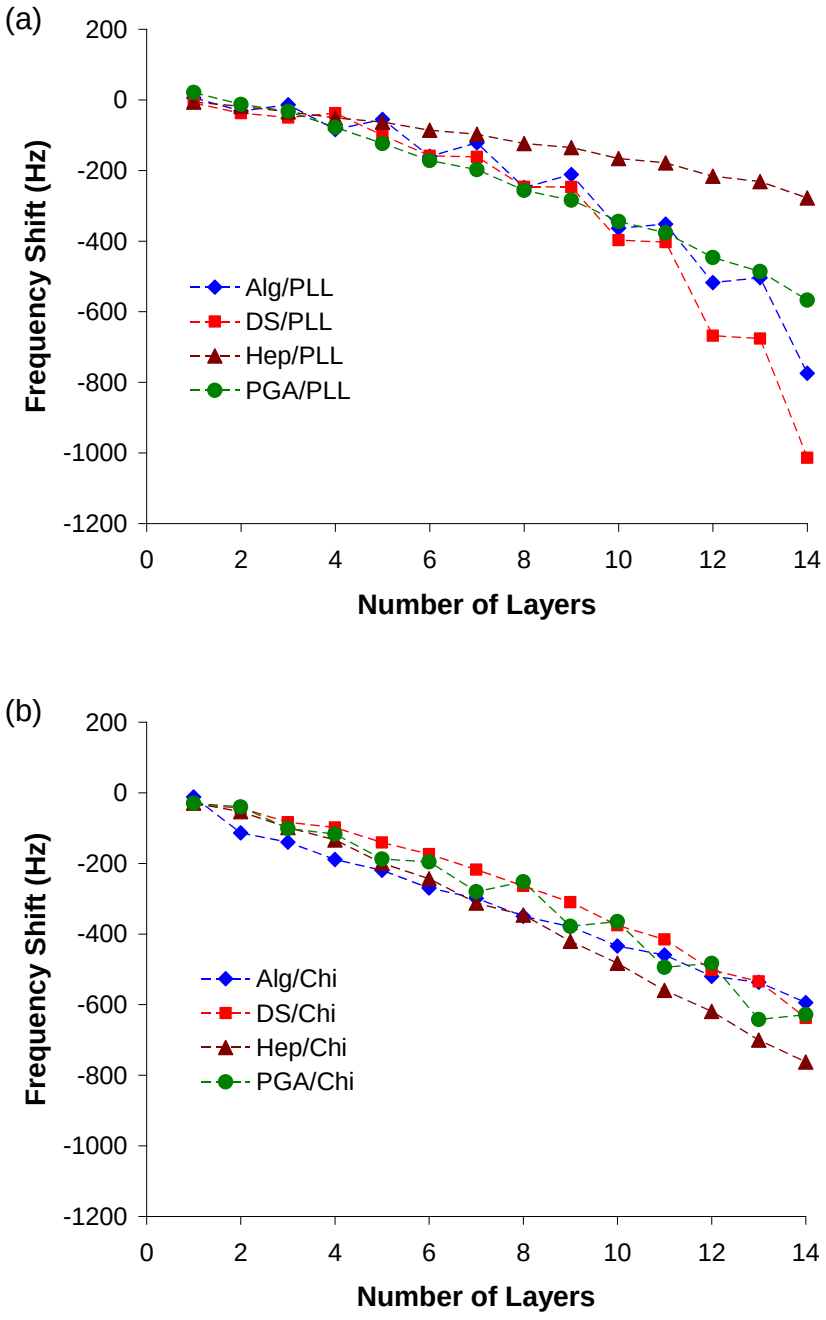

Figure 27. Cumulative QCM frequency shifts (ΔF) of (a) polyanions/PLL adsorption and (b) polyanions/Chi adsorption on the gold coated quartz crystal electrode. Odd numbers of layers represent either PLL or Chi and even numbers of layers represent polyanions.

Table 6. Thickness (*L*) and static contact angle (*CA*) measurements of 6.5 and 7 bilayers of each BPEM component. ( ) indicates 95% confidence interval (n=15 for *L* and n=3 for *CA*).

BPEMs	***L (nm)***		***CA (°)***	
	6.5 bilayers	**7 bilayers**	**6.5 bilayers**	**7 bilayers**
[Alg/PLL]	140 (± 7.2)	133 (± 12.1)	61 (± 3.7)	58 (± 1.7)
[DS/PLL]	134 (± 4.9)	135 (± 4.0)	8 (± 1.4)	17 (± 1.6)
[Hep/PLL]	103 (± 2.6)	117 (± 4.1)	41 (± 2.5)	52 (± 1.2)
[PGA/PLL]	103 (± 19.9)	118 (± 14.9)	70 (± 1.9)	72 (± 0.4)
[Alg/Chi]	41 (± 5.0)	54 (± 9.1)	39 (± 4.8)	44 (± 5.9)
[DS/Chi]	78 (± 11.6)	101 (± 5.7)	13 (± 1.4)	18 (± 1.6)
[Hep/Chi]	117 (± 4.2)	126 (± 8.6)	14 (± 1.0)	16 (± 4.2)
[PGA/Chi]	41 (± 5.8)	72 (± 9.1)	31 (± 1.5)	31 (± 2.1)

Contact angles of each film also vary with different combinations of films (Table 6), and each film has unique transport properties to glucose (Figure 28). It is generally believed that a high degree of film wettability increases permeation of water-soluble substances as well as promotes water flux.[89, 93] However, we found that glucose permeation rates of corresponding films are not directly correlated with their surface wettability ($\rho(CA, dC/dt) = -0.72$). For example, both DS/Chi and Hep/Chi represent higher *dC/dt* relative to DS/PLL with similar low contact angles. As with most synthetic polyelectrolyte multilayers, many factors such as polyelectrolyte concentration,

temperature, degree of interdiffusion, pH, and ionic strength may influence the nanoporosity of multilayer films.

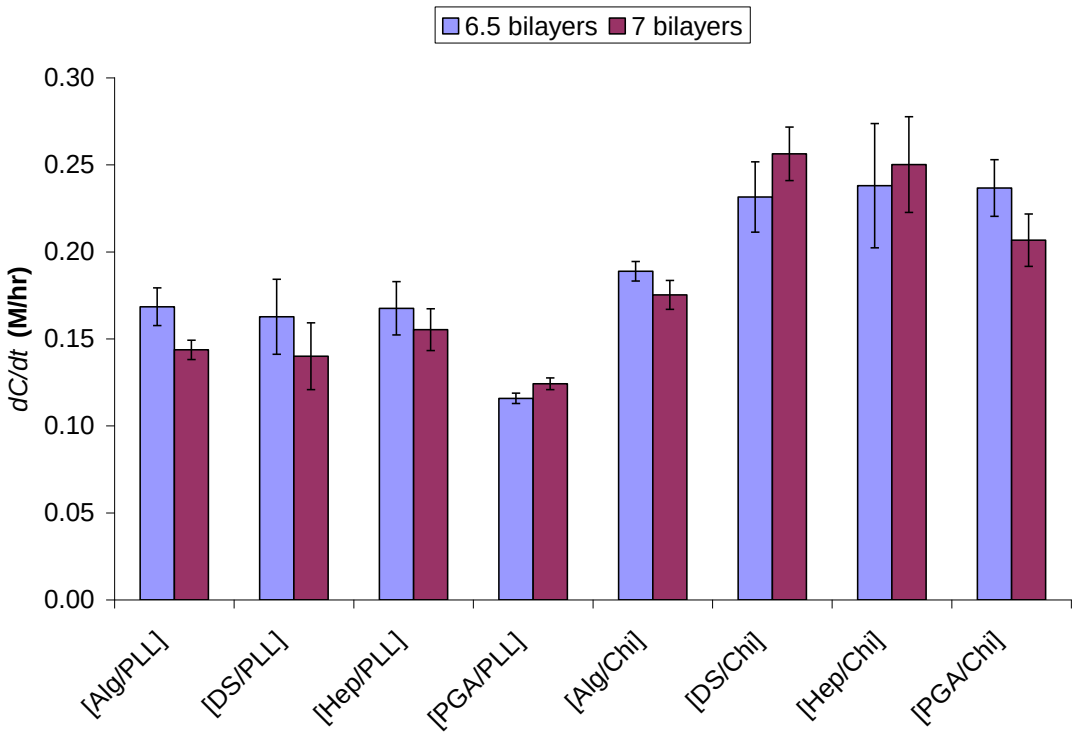

Figure 28. Permeate concentrations of glucose through the films were measured as a function of time (*dC/dt*). Error bars indicate 95% confidence interval (n=3).

Crosslinking of polyelectrolyte multilayers has been extensively applied for drug delivery,[94] stability of PEMs over a wide range of pH values,[95, 96] and modulating

mechanical properties.[97] Chemical crosslinking between carboxylic groups and amine groups inside the multilayer structure forms amide bonds.[86] This protocol was based on carbodiimide (EDC) chemistry, which used a "zero length" crosslinker in salt-containing medium at mild temperature, and can be applied to any type of polyelectrolyte multilayers that possess carboxylic and primary amine groups. Crosslinking of Alg/PLL, Hep/PLL, PGA/PLL, Alg/Chi, Hep/Chi, and PGA/Chi were examined using attenuated total reflectance Fourier transform infrared spectroscopy (ATR-FTIR). All PLL-based nanofilms showed increased absorbance at around 1650 cm^{-1} (primary amide peak)[86] after crosslinking of the nanofilms (Figure 29). However, Chi-based BPEMs exhibited decreased absorbance at the same wavenumber, 1650 cm^{-1} (Figure 30). In general, strong intramolecular hydrogen bonding with aldehydes, ketones, or esters appears at 1630-1670 cm^{-1}. We interpret our findings as showing that hydrogen bonding in Chi-based materials was displaced after crosslinking of BPEMs.

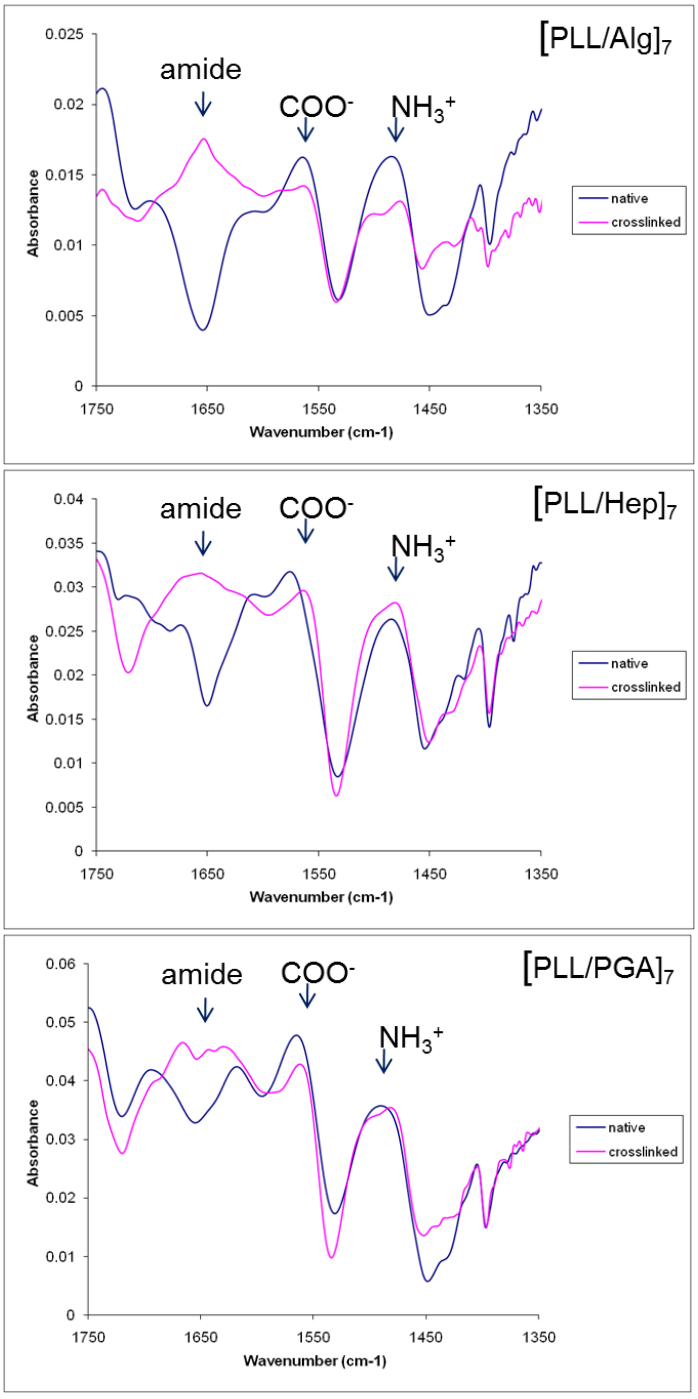

Figure 29. ATR FT-IR spectra of $[PLL/Alg]_7$, $[PLL/Hep]_7$, and $[PLL/PGA]_7$ before and after crosslinking of BPEMs.

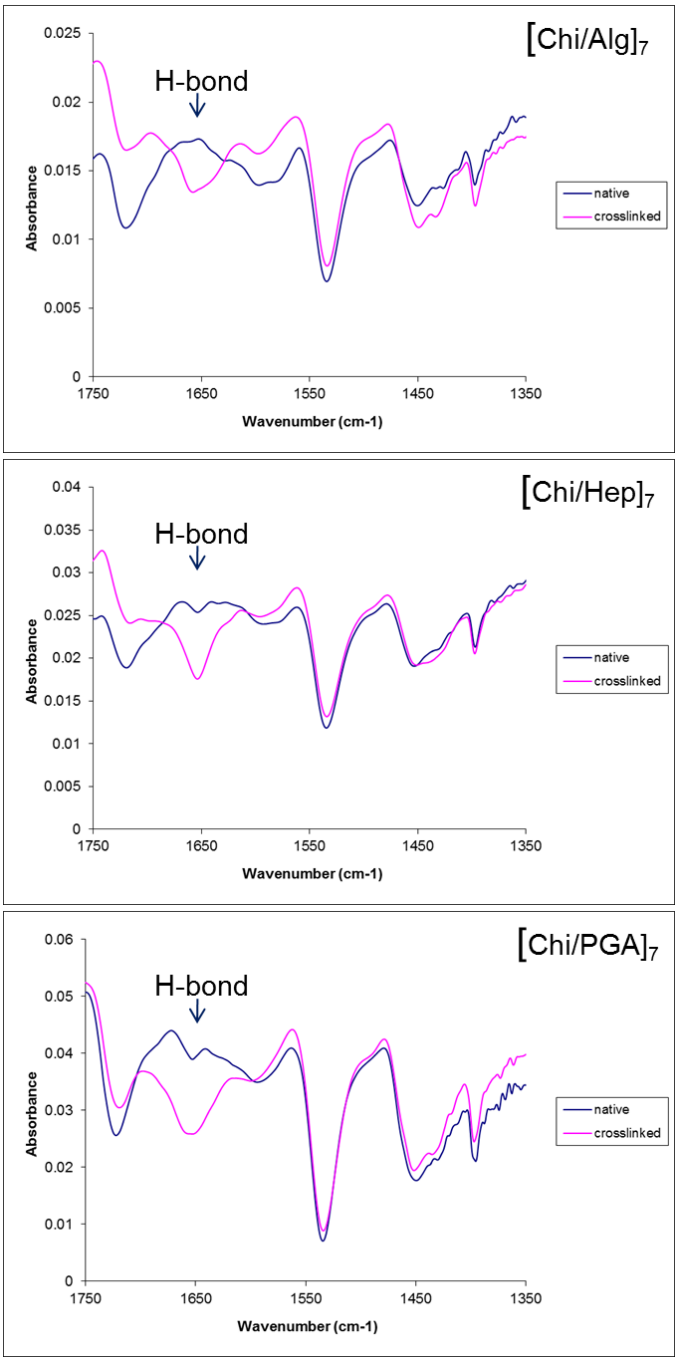

Figure 30. ATR FT-IR spectra of $[Chi/Alg]_7$, $[Chi/Hep]_7$, and $[Chi/PGA]_7$ before and after crosslinking of BPEMs.

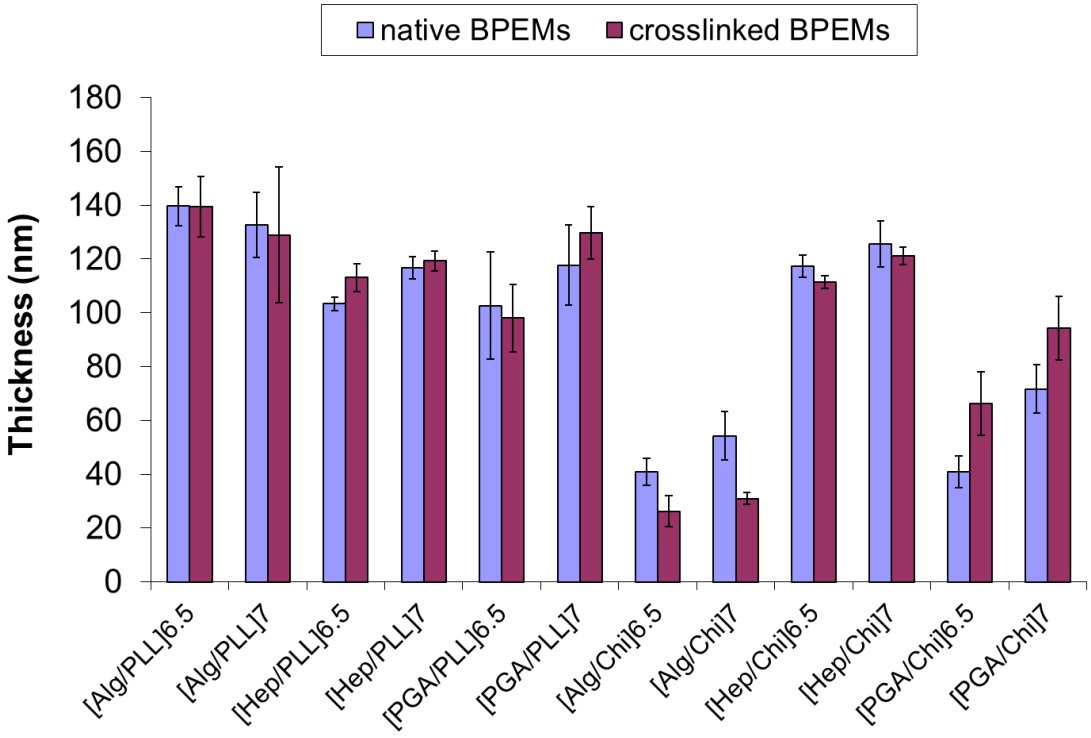

Figure 31. Nanofilm thickness before and after crosslinking of BPEMs measured by ellipsometry. Error bars represent 95% confidence interval (n=15).

Thickness of each film was compared before and after crosslinking of BPEMs (Figure 31). No statistical difference was observed after crosslinking in most cases, except Alg/Chi and PGA/Chi. Interestingly, the thickness of the PGA/Chi film increased up to 61% after crosslinking, while the Alg/Chi film decreased up to 43%. It is highly possible that structural changes of biopolymers occurred during crosslinking. Boulmedias et al. and Pilbat and coworkers reported that polyelectrolyte multilayers,

especially constructed with polypeptides, represent secondary structures (α-helix and β-sheet) that assume different conformations in different environments (e.g. polyelectrolyte pair, temperature, solvent, pH, etc.).[98, 99] Boudou et al. reported that poly(allylamine hydrochloride)/PGA (PAH/PGA) films have the most dense structure and the highest density of carboxylic groups relative to other biopolyelectrolytes such as PLL/hyaluronan (PLL/HA) and Chi/hyaluronan (Chi/HA),[100] which suggests that PGA has greater capacity for crosslinking. These results indicate that crosslinking in certain pairs of polyelectrolytes induces a conformational change of the multilayer structure. Surface wettability of multilayer films also exhibited different trends among various film pairs (Figure 32). Hydrophobicity increased in most Chi-based film structures after crosslinking; on the other hand, PLL-based films preserved statistically the same or less contact angle after crosslinking. For example, PGA/PLL exhibited significantly decreased contact angle, while Hep/Chi and PGA/Chi exhibited increased contact angles after crosslinking. Also, for Alg/PLL and Hep/PLL, contact angles for 6.5 bilayers were statistically different after crosslinking, while no difference for 7 bilayers was observed (α=0.05).

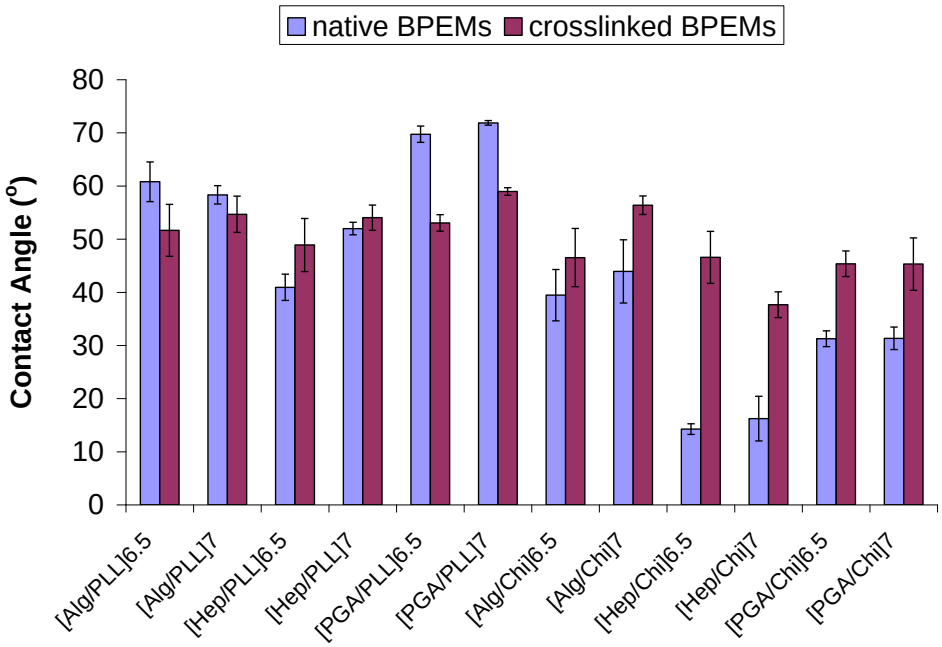

Figure 32. Static (Θ_{static}) contact angles of nanofilms before and after crosslinking of BPEMs. Error bars indicate 95% confidence interval (n=3).

As mentioned previously, crosslinking of biopolyelectrolyte multilayers has many advantages. However, to our best knowledge, no comparison of film permeability before and after crosslinking of biopolyelectrolyte multilayer films has been performed. The change in permeability after crosslinking of multilayer films was studied and was determined to be the result of changing film characteristics.

Significant decreases in permeability were observed in Hep/Chi and PGA/Chi pairs (up to 47% decrease in $[Hep/Chi]_7$) after crosslinking of BPEMs (Figure 33). These results indicate that one of the major factors in changing the permeation rate of crosslinked films is water wettability of the surface. As discussed earlier, increasing hydrophobicity decreases permeation of water soluble substances in general. All

crosslinked Hep/Chi and PGA/Chi pairs decreased the permeation rate up to 47% relative to native multilayer films, with accompanying significant increases in contact angles of the corresponding film pairs. However, either increasing or decreasing trends of permeability with other pairs of crosslinked BPEMs were not governed by the surface wettability of the BPEMs ($\rho(CA, dC/dt) = -0.44$). It should also be pointed out that statistically equivalent glucose permeation was observed in many BPEM pairs after crosslinking (e.g. $[Alg/PLL]_{6.5}$, $[Alg/PLL]_{7}$, $[Hep/PLL]_{6.5}$, $[PGA/PLL]_{6.5}$, $[Alg/Chi]_{6.5}$, and $[Alg/Chi]_{7}$).

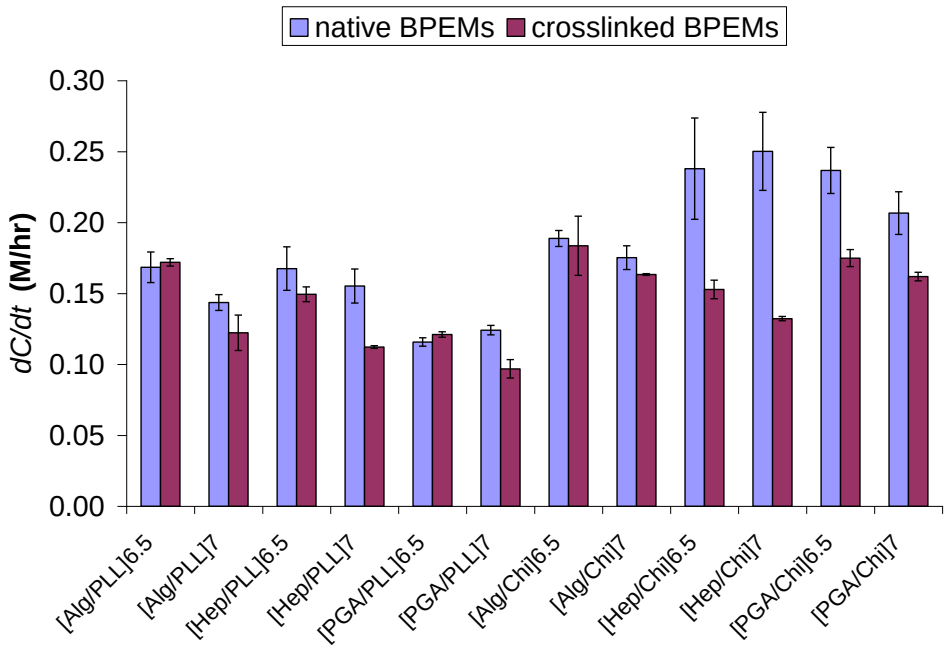

Figure 33. Permeation rate (*dC/dt*) of glucose through various BPEMs before and after chemical crosslinking. Error bars indicate 95% confidence interval (n=3).

Diffusion coefficients (*D* values) of glucose through all the BPEMs, including crosslinked films, were calculated based on experimentally-measured thicknesses and permeation rates (*dC/dt*) (Table 7). The *D* values of BPEMs were up to four orders of magnitude lower than the *D* value of bare substrate (1.15×10^{-6} cm^2/sec). However, these values are still one or two orders of magnitude higher than the previous reported *D* values of synthetic polyelectrolyte multilayers such as PSS/PAH and PAA/PAH.[101]

Table 7. Diffusion coefficients (*D*) of glucose through various BPEMs were extracted by regression of flux and concentration gradient data using *Fick's* law. Note: *D* value through bare substrate is 1.15×10^{-6} cm^2/sec. ( ) indicates 95% confidence interval (n=3).

BPEMs	***D* (X 10^{-10} cm^2/sec)**			
	native BPEMs		**crosslinked BPEMs**	
	6.5 bilayers	**7 bilayers**	**6.5 bilayers**	**7 bilayers**
[Alg/PLL]	24.8 (± 1.5)	20.1 (± 2.2)	24.9 (± 4.5)	16.5 (± 5.7)
[DS/PLL]	23.0 (± 3.7)	19.9 (± 3.1)	n/a	n/a
[Hep/PLL]	18.3 (± 1.4)	19.1 (± 0.9)	17.9 (± 2.1)	14.1 (± 0.6)
[PGA/PLL]	12.5 (± 0.4)	15.2 (± 0.1)	12.2 (± 1.5)	12.7 (± 1.1)
[Alg/Chi]	8.2 (± 1.0)	10.0 (± 2.9)	4.4 (± 0.3)	5.4 (± 0.1)
[DS/Chi]	19.1 (± 1.7)	27.4 (± 1.6)	n/a	n/a
[Hep/Chi]	29.4 (± 3.7)	33.5 (± 8.6)	17.7 (± 0.4)	17.1 (± 0.7)
[PGA/Chi]	10.3 (± 3.0)	15.7 (± 4.4)	10.6 (± 3.9)	16.2 (± 3.2)

5.4. Conclusions

During the last decade, there has been considerable development in the field of biomimetic self-assembly with developing PEM films from biomaterial surfaces.[85] The potentialities for constructing biofunctional coatings that limit transport of small molecules are attractive. Regarding the transport control of small molecules over the PEM films, synthetic PEMs have been widely investigated.[29, 101] However, a study of the transport properties of biologically-relevant materials has been less considered.

The construction of biological polyelectrolyte multilayers was investigated at the nanometer scale in a physiological environment, and diffusion properties of glucose through each BPEM were determined. *D* values of glucose through all the BPEMs, including native and crosslinked films, were three to four orders of magnitude lower than the *D* value of bare substrate in all cases; however, these *D* values are one or two orders of magnitude higher than the previously reported *D* values of synthetic polyelectrolyte multilayers such as PSS/PAH and PAA/PAH. Permeation rates (*dC/dt*) of all BPEMs were up to 2 orders of magnitude higher than the [PAA/PAH]-based film. Crosslinking BPEMs decreased diffusivity of glucose by up to 51% as compared to the native BPEMs. The permeability of BPEMs mainly depends on the component materials of BPEMs, and no general trends governing correlation of film characteristics (i.e. contact angle, thickness, and crosslinking) and permeation rate were observed.

Specific applications for BPEM coatings can be followed by *in vivo* clinical studies such as biodegradation, biostability, and biofouling.[85] Our findings of the

transport properties of biological multilayer films can also be applied in drug delivery, cell systems, and tissue engineering.

6. MULTI-PHASE NANOCOMPOSITE FILMS: THEORETICAL AND MEASURED PERMEABILITIES

6.1. Introduction

Nanocomposite polymeric materials have attention in a variety of fields including bio/chemical sensing, drug delivery, biomimetic surfaces, mechanical actuations and separations.[102-106] We have already determined the glucose diffusion coefficient for each nanocomposite (bi-component) film throughout the previous sections. We hypothesized that integrating those nanocomposite films based on all the known properties of the individual components can yield multi-phase nanocomposite films with desirable diffusivity and interfacial properties for specific applications. For example, we can construct nanoscale composite films that contain a diffusion-limiting inner layer with a biological outer layer. It is also possible that we may predict the analyte permeation rate through the multi-phase nanocomposite films of known diffusivity for selection and design of functional transport-controlling materials.

In this section, using measurement data from bi-component nanofilms and the generalized theoretical description, prediction of properties of more complex multi-component systems were used to design membranes with desirable transport properties. Additional nanofilm membranes comprised of combinations of characterized bi-component films were assembled onto the substrate and glucose diffusion profiles were obtained. Given the previously extracted nanocomposite diffusion coefficients, the

theoretical permeation rates were determined using the modeling procedure and directly compared to experimental results. To our knowledge, there has been no work toward an approach that allows prediction of diffusion properties of multi-phase nanoscale composite membranes; thus, should this approach yield reasonably accurate estimates, a significant contribution to nanofilm transport profile would be introduced.

6.2. Materials and Methods

6.2.1. Theoretical calculations of dC/dt for multi-phase nanocomposite films

A two-phase nanocomposite membrane comprised of two different nanocomposite membranes, each with thickness L_1 and L_2 and diffusion coefficient D_1 and D_2, where the amount of substance diffused through Membrane 1 will be the amount of substance entering Membrane 2, is depicted in Figure 34.[39]

For one-dimensional steady-state diffusion

$$\frac{d^2C}{dx^2} = 0$$

The above equation is valid for both phases. Thus, we have two problems with two solutions:

$$C_1 = A_1 + B_1x$$

$$C_2 = A_2 + B_2x$$

There are four constants of integration—$A_1, A_2, B_1, and\ B_2$—and four boundary conditions are given. Variables were defined in Section *2.2.5.*:

$$x = 0 \quad C_1 = \Phi_1 C_0$$

$$x = L \quad C_2 = \Phi_2 C_L$$

The other two conditions are at $x = L_1$, where $C_1/\Phi_1 = C_2/\Phi_2$ and $J_1 = J_2$

Applying condition at $x = 0$ yields $A_1 = \Phi_1 C_0$. From the second boundary condition, we get $A_2 = \Phi_2 C_L - B_2 L$. Next we apply the above equation to yield the following:

$$C_0 + B_1 L_1/\Phi_1 = C_L + B_2 L_2/\Phi_2\ ,\ D_1 B_1 = D_2 B_2$$

Solving for the unknowns yields an expression for the concentration profiles and the flux:

$$0 < x < L_1 \quad C_1 = \Phi_1 C_0 - \frac{D_2 \Phi_1 \Phi_2 (C_0 - C_L) x}{D_2 \Phi_2 \Phi_1 + D_2 \Phi_1 \Phi_2}$$

$$L_1 < x < L_2 \quad C_2 = \Phi_2 C_L - \frac{D_1 \Phi_1 \Phi_2 (C_0 - C_L)(x - L)}{D_2 \Phi_2 \Phi_1 + D_1 \Phi_1 \Phi_2}$$

$$J_1 = J_2 = \frac{D_1 D_2 \Phi_1 \Phi_2 (C_0 - C_L)}{D_2 \Phi_2 L_1 + D_1 \Phi_1 L_2}$$

The flux is independent of location in the region between $x = 0\ and\ x = L$. For a single phase medium, $D_1 = D_2$. The flux can be rewritten as

$$J_1 = J_2 = \frac{\Phi D}{L}(C_0 - C_L)$$

from which follows that

$$\frac{L}{\Phi D} = \frac{L_1}{\Phi_1 D_1} + \frac{L_2}{\Phi_2 D_2}$$

where Φ is the partition coefficient.

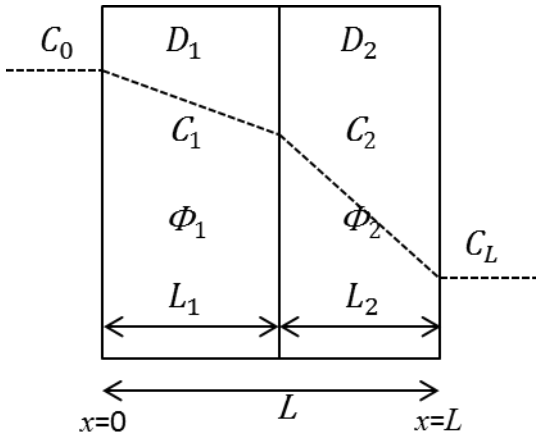

Figure 34. Diffusion of small molecules through two-phase nanocomposite film model.

Based on the estimated thickness and *D* values on Table 8, we can extract *D* values for multi-phase nanocomposite films by again assuming partition coefficient (Φ) of all phases are unity (as discussed this in Section *2.2.5.*).

The relation of permeation rate (*dC/dt*) and *D* (as described in Section *2.2.5.*) is:

$$-V_1 \frac{dC_1}{dt} = A_m D_m \Phi \frac{(2C_1 - C_0)}{L}$$

Thus, we can obtain the theoretical *dC/dt* from the above relation.

$$\frac{dC}{dt} = D \frac{\Phi C_0}{lL}$$

6.2.2. Materials

We determined permeation rates (*dC/dt*) of various bi-component nanofilms, as reported in Sections 2–5 (Figure 35). From these data, we selected five pairs of bi-component films based on material category and permeation rate (Table 8). To observe the role of each bi-component film within a multi-phase nanocomposite, we selected the combinations comprising bi-component nanocomposite films with different permeabilities. Candidate bi-component nanocomposite films are high and low *dC/dt* pairs from the synthetic polyelectrolyte multilayers (PEMs), and high, medium, and low *dC/dt* pairs from the biopolyelectrolyte multilayers (BPEMs).

Poly(styrene sulfonate) (*PSS*, M_w~70,000), poly(acrylic acid) (*PAA*, M_w~100,000, 35 wt. % in water), poly(allylamine hydrochloride) (*PAH*, M_w~70,000) Poly-L glutamic acid sodium salt (*PGA,* M_v=15,000-50,000), and chitosan (*Chi,* M_w ~ 50,000) were purchased from Aldrich. Glucose, poly-L-lysine hydrobromide (*PLL,* M_w=15,000-30,000), alginic acid sodium salt (*Alg*) from brown algae, glucose oxidase, peroxidase, *o*-dianisidine, NaCl, NaOH, HCl, and phosphate buffered saline (PBS) were purchased from Sigma. Dextran sulfate sodium salt (*DS*, M_w>500,000) was purchased from Sigma-Aldrich. The porous alumina supports (Anodisc 25, 0.02μm pore diameter) were purchased from Whatman Ltd. Deionized water (>18.2 MΩcm) was always used for preparation of polyelectrolyte solutions and rinsing. The pH of the polyelectrolyte solutions was adjusted with either HCl or NaOH.

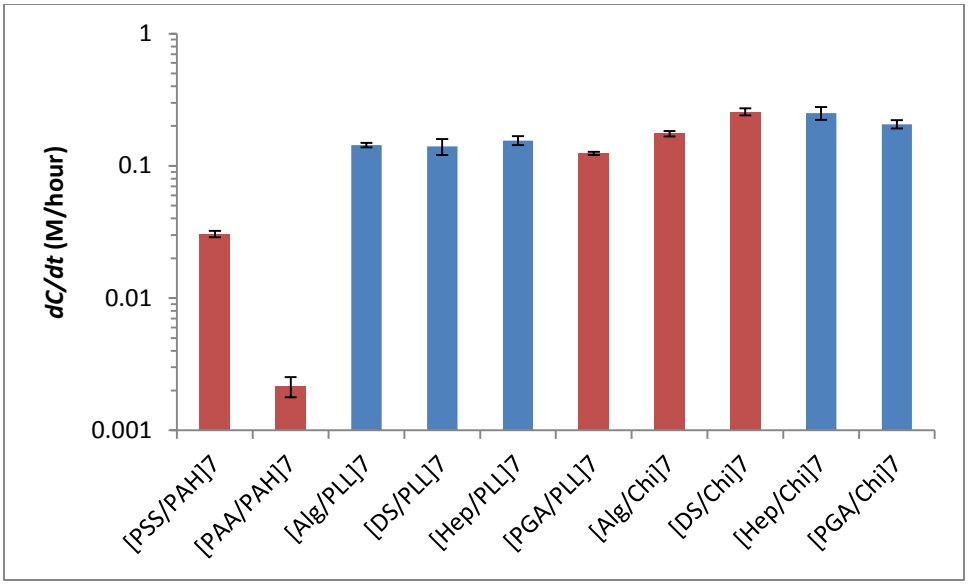

Figure 35. Measured permeation rates (*dC/dt*) of bi-component nanocomposite films. These data were compiled from Section 2 and Section 5. Error bars indicate 95% confidence interval (n=3).

Table 8. Selected bi-component nanocomposite films.

Bi-component film	Description	Measured $L_{7\text{-bilayer}}$ (nm)	$\Delta F_{3\text{-bilayers}} / \Delta F_{7\text{-bilayers}}$	Estimated $L_{7\text{-bilayer}}$ [a] (nm)	Estimated D [b] (cm^2/sec)
$[PSS/PAH]_3$	Synthetic PEM w/ high *dC/dt* **(SynH)**	77	0.44	34	3.93×10^{-10}
$[PAA/PAH]_3$	Synthetic PEM w/ low *dC/dt* **(SynL)**	108	0.11	12	2.61×10^{-11}
$[DS/Chi]_3$	Biological PEM w/ high *dC/dt* **(BioH)**	101	0.27	28	2.74×10^{-9}
$[Alg/Chi]_3$	Biological PEM w/ medium *dC/dt* **(BioM)**	54	0.45	25	9.99×10^{-10}
$[PGA/PLL]_3$	Biological PEM w/ low *dC/dt* **(BioL)**	118	0.30	36	1.52×10^{-9}

a. Thickness of three bilayers were estimated using QCM data:
$L_{\text{estimated}} = L_{7\text{-bilayer}} \times \Delta F_{3\text{-bilayers}} / \Delta F_{7\text{-bilayers}}$ (refer Section 2 and Section 5).
b. Assume *D* values through 3-bilayers are same as *D* values through 7-bilayers.

6.2.3. Layer-by-layer self-assembly

Multi-phase nanocomposite films were constructed by various combinations of bi-component films. Film deposition followed previous Sections (*2.2.2., 5.2.2.*). PSS/PAH deposition started with exposure of one side of the alumina support using open-face filter holders (Pall Co.) in 0.02 M PSS in 0.5 M NaCl solution adjusted to pH 2.1 for 5 min. The alumina support was rinsed with deionized water for 1 min before exposure to 0.02M PAH in 0.5 M NaCl adjusted to pH 2.3 for 5 min, followed by another water rinse for 1 min. PAA/PAH alternative adsorption involved the same deposition and rinse time with 0.02M PAA (pH 5.5, 0.5 M NaCl) and 0.02 M PAH (pH 5.5, 0.5 M NaCl). This process was repeated until the target number of layers was achieved without drying between each step.

PGA/PLL depositions started with exposure of one side of the alumina support using an open-face filter holder (Pall Co.) in 1 mg/mL PGA in PBS for 10 min. The film was rinsed with PBS for 1 min before exposure to 1 mg/mL PLL in PBS for 10 min, followed by another PBS rinse for 1 min. Chitosan-based LbL (DS/Chi or Alg/Chi) adsorptions involved 10 min deposition with 1mg/mL of each polyanion in 0.15 M NaCl solutions adjusted to pH 5.5 and 1 mg/mL chitosan in 0.15 M NaCl solution adjusted to pH 5.5. All chitosan-based multilayers were rinsed with 0.15 M NaCl during the LbL self-assembly. We repeated this process until the target number of layers was achieved.

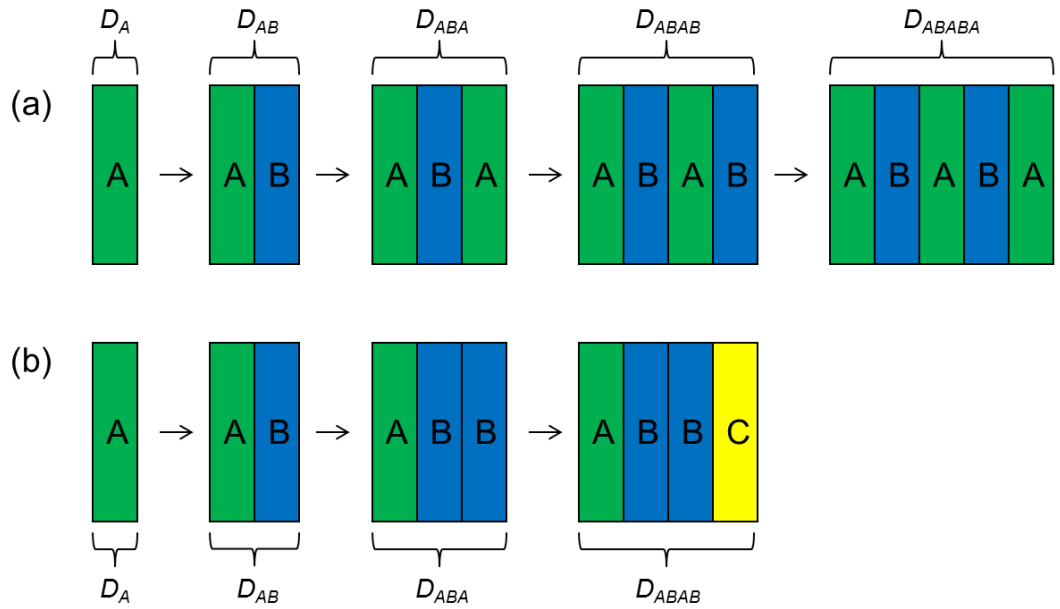

Figure 36. Illustration depicting the representation of multi-phase nanocomposite films comprised of combinations of previously characterized bi-component films (A, B, and C). (a) represents a two-phase alternative nanocomposite film and (b) represents a three-phase nanocomposite film.

6.2.4. Diffusion measurements and calculation of experimental diffusivity

Diffusion of glucose through multi-phase nanocomposite films were measured using the same experimental system described in Section *2.2.4.*. Calculation of glucose diffusivity followed the mathematical method described in Section *2.2.5.*.

6.3. Results and Discussion

The LbL process was applied with various combinations of bi-component films. The permeation rates (*dC/dt*) were extracted theoretically (see Section *6.2.2.*) and experimentally. $[DS/Chi]_3$ (biological PEM with high *dC/dt*) and $[PGA/PLL]_3$ (biological PEM with low *dC/dt*) were alternatively assembled, and there was no statistical difference between $[DS/Chi]_3$ (A) and $[DS/Chi]_3[PGA/PLL]_3[DS/Chi]_3[PGA/PLL]_3$ (ABAB) in permeation rate (Figure 37). Overall $[DS/Chi]_3[PGA/PLL]_3[DS/Chi]_3[PGA/PLL]_3[DS/Chi]_3$ (ABABA) has 77% of *dC/dt* compared to initial $[DS/Chi]_3$. However, as discussed in Section 5, biological PEMs do not dramatically limit the glucose permeation compared to synthetic PEMs.

Figure 38 shows the permeation rate for sequential adsorption of $[PSS/PAH]_3$ (synthetic PEM with high *dC/dt*) and $[PAA/PAH]_3$ (synthetic PEM with low *dC/dt*). The permeation rate was significantly decreased by a factor of six after addition of $[PAA/PAH]_3$ (AB) on top of $[PSS/PAH]_3$ and no statistical difference was observed with another addition of $[PSS/PAH]_3$ (ABA) (α=0.05). The next addition of $[PAA/PAH]_3$ (ABAB) decreased the permeation rate again by a factor of two and no difference was observed with another addition of $[PSS/PAH]_3$ (ABABA).

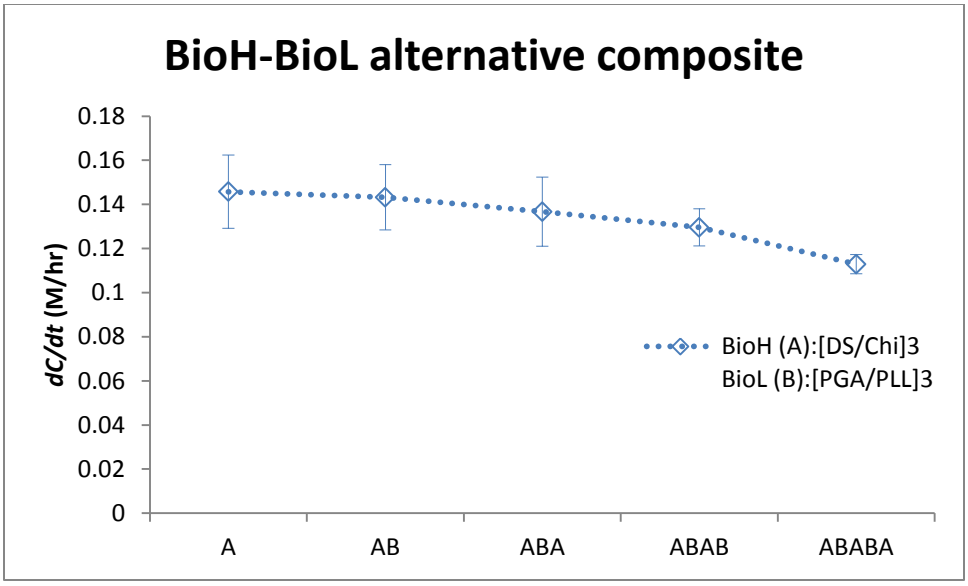

Figure 37. Permeation rates (*dC/dt*) of glucose through nanocomposite films of $[DS/Chi]_3$ (A, BioH) and $[PGA/PLL]_3$ (B, BioL). All error bars indicate 95% confidence interval based on n=3 replicate samples.

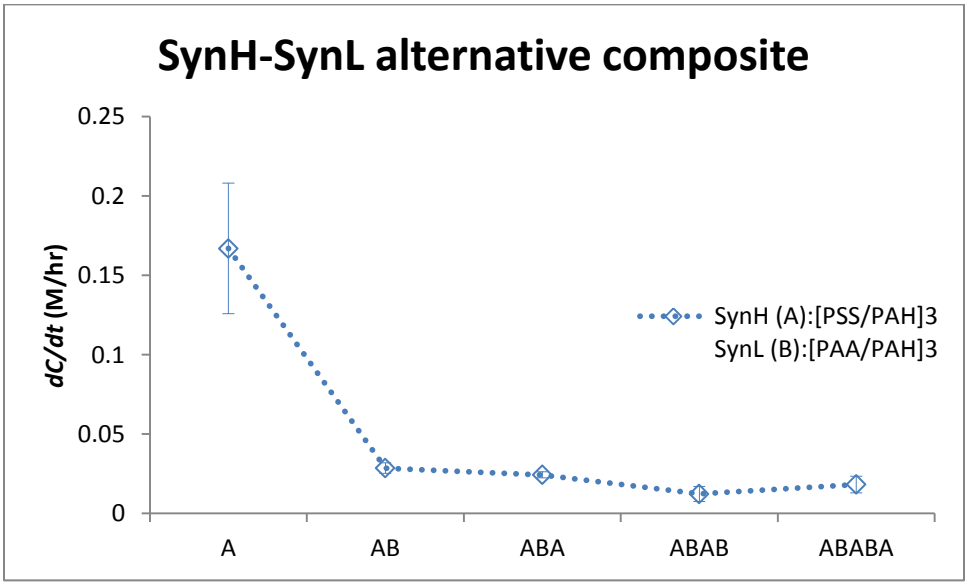

Figure 38. Permeation rates (*dC/dt*) of glucose through nanocomposite films of $[PSS/PAH]_3$ (A, SynH) and $[PAA/PAH]_3$ (B, SynL). All error bars indicate 95% confidence interval based on n=3 replicate samples.

After separate investigations of biological and synthetic multi-phase nanocomposite systems, we combined these systems to maximize the utility of coatings in biomedical applications. For example, synthetic PEMs provide greater transport-limiting properties, whereas biological PEMs can exhibit bio-interfacial functionality in a physiological environment.

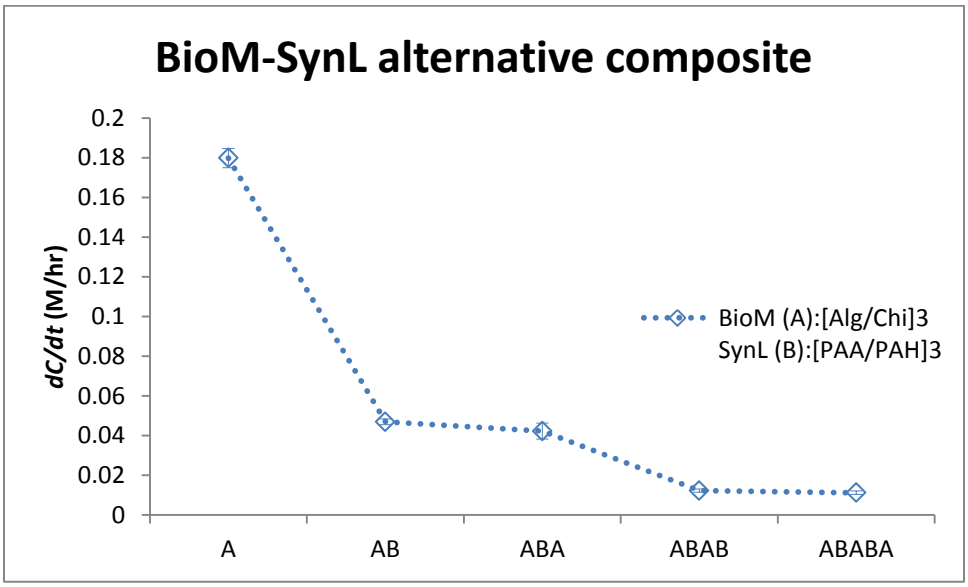

Figure 39. Permeation rates (*dC/dt*) of glucose through nanocomposite films of $[Alg/Chi]_3$ (A, BioM) and $[PAA/PAH]_3$ (B, SynL). All error bars indicate 95% confidence interval based on n=3 replicate samples.

$[Alg/Chi]_3$ and $[PAA/PAH]_3$ were selected as a biological PEM with medium *dC/dt* and a synthetic PEM with the lowest *dC/dt,* respectively. It was observed that [Alg/Chi] did not play a role to limit diffusion relative to [PAA/PAH] as expected (Figure 39). It must be pointed out that three bilayers of either nanofilm—biological or synthetic PEM—are not enough to limit glucose transport due to the lack of surface coverage. Interestingly, all initial three bilayer films exhibited the same *dC/dt* values (α=0.05), regardless of whether the PEM is synthetic or biological (Figure 42).

After investigations of various two-phase nanocomposite systems (Figure 36 a), we constructed three-phase nanocomposite films (Figure 36 b) with various combinations of bi-component films. As observed previously, the [PAA/PAH] film exhibited the lowest permeation of glucose. It was hypothesized that a "PAA/PAH sandwich"—a PAA/PAH film between two other bi-component films—could significantly limit diffusion, while providing desired functionality on both interfaces. This can maximize the utility of these nanocomposite films in applications such as coatings of biomedical devices. For example, while PAA/PAH possesses great diffusion-limiting behavior (refer to Section 4), its diffusion behavior is susceptible to modification in the presence of proteins or serum. Combining PAA/PAH with BPEMs or a stable outer film such as PSS/PAH will improve the functionality or stability of the nanofilm coating, respectively.

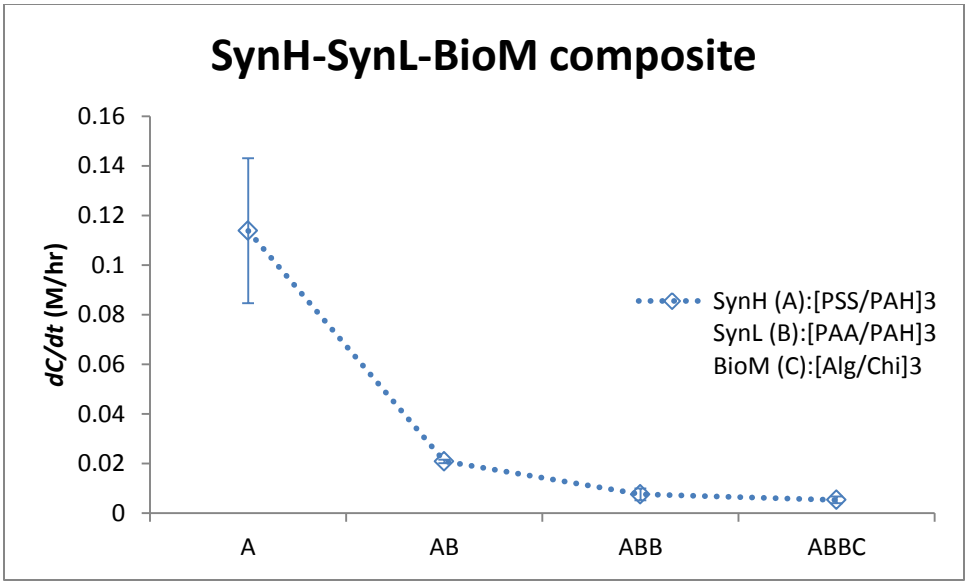

Figure 40. Permeation rates (*dC/dt*) of glucose through nanocomposite films of $[PSS/PAH]_3$ (A, SynH), $[PAA/PAH]_3$ (B, SynL), and $[Alg/Chi]_3$ (C, BioM). All error bars indicate 95% confidence interval based on n=3 replicate samples.

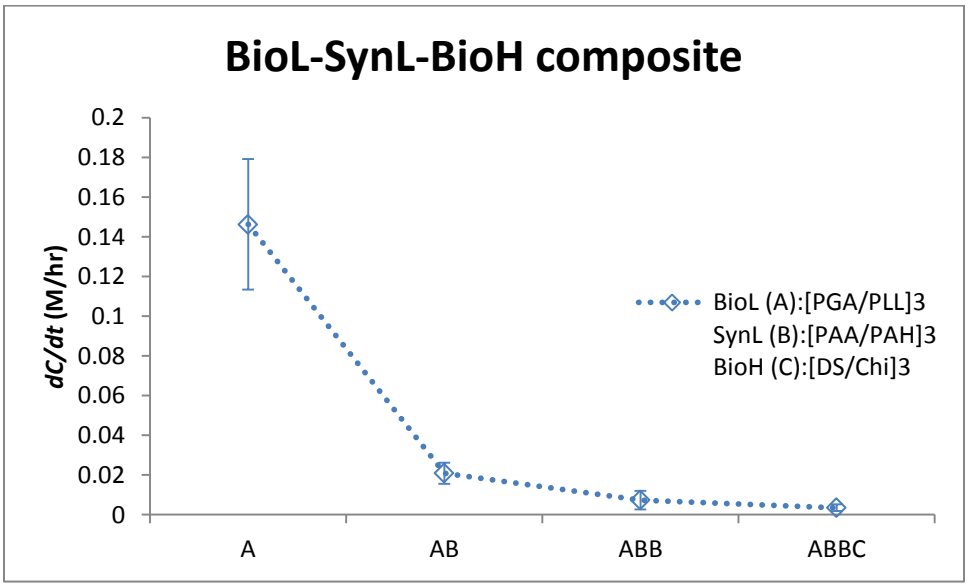

Figure 41. Permeation rates (*dC/dt*) of glucose through nanocomposite films of $[PGA/PLL]_3$ (A, BioL), $[PAA/PAH]_3$ (B, SynL), and $[DS/Chi]_3$ (C, BioH). All error bars indicate 95% confidence interval based on n=3 replicate samples.

Permeation rates of sequential adsorption of $[PSS/PAH]_3$, $[PAA/PAH]_3$, and $[Alg/Chi]_3$ are shown in Figure 40. Another set of three-phase nanocomposite films composed of adsorption of $[PGA/PLL]_3$, $[PAA/PAH]_3$, and $[DS/Chi]_3$ were also tested (Figure 41). As expected from previous data, it was confirmed that PAA/PAH played a major role as a diffusion-limiting layer in both types of three-phase nanocomposite films regardless of the outer bi-component films (Figure 42).

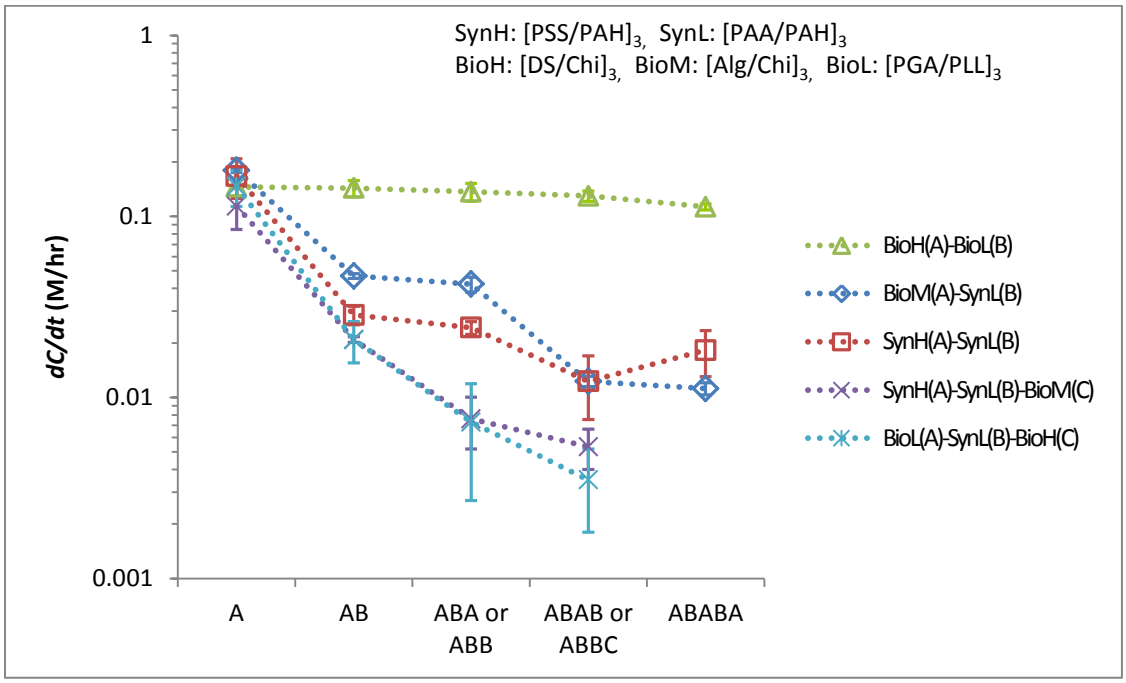

Figure 42. Compiled permeation rates (*dC/dt*) of multi-phase nanocomposite films composed of various combinations of bi-component films. All error bars indicate 95% confidence interval based on n=3 replicate samples.

We examined our prediction approach of permeation rate by using estimated parameters (*L* and *D* in Table 8) and the equation described in Section *6.2.2.*. These values were compared with the experimental permeation rate of the overall multi-phase nanocomposite films (ABABA or ABBC structure) obtained from the diffusion cell experiments (Figure 43). The predicted *dC/dt* values of multi-phase nanocomposites of {[PSS/PAH]$_3$-[PAA/PAH]$_3$} and {[PGA/PLL]$_3$-[PAA/PAH]$_3$-[DS/Chi]$_3$} do not match with experimental *dC/dt* values of corresponding films (α=0.05). However, the theoretical values of multi-phase nanocomposites of {[Alg/Chi]$_3$-[PAA/PAH]$_3$}, {[DS/Chi]$_3$-[PGA/PLL]$_3$}, and {[PSS/PAH]$_3$-[PAA/PAH]$_3$-[Alg/Chi]$_3$} accurately predicted the experimental *dC/dt* values (no significant difference at α=0.05).

In this approach, the fundamental assumptions of the relation of *dC/dt* and *D* are that the multi-phase transport-limiting nanofilms behave like a classical laminate structure. However, a major issue in quantifying nanofilm permeability and utilization of the models described in Section *6.2.2.* is the assessment of the three parameters (*L*, Φ, *D*) defining nanofilm permeability. For example, the thickness in the dry condition may be different in the hydrated condition. Partitioning behavior in an intricate composite structure might be another major factor to differentiate modeling values and experimental values. The required parameters may vary depending on the complexity of composite structure (e.g. local chemistry, polymer chain mobility, conformation, and crystalinity),[107] especially in the inter-penetrated polymer structure as described in Section *6.1.*. Based on our modeling and experimental data, it must be pointed out that the ratios of experimental to predicted *dC/dt* values are within the range of 0.35 – 2.39.

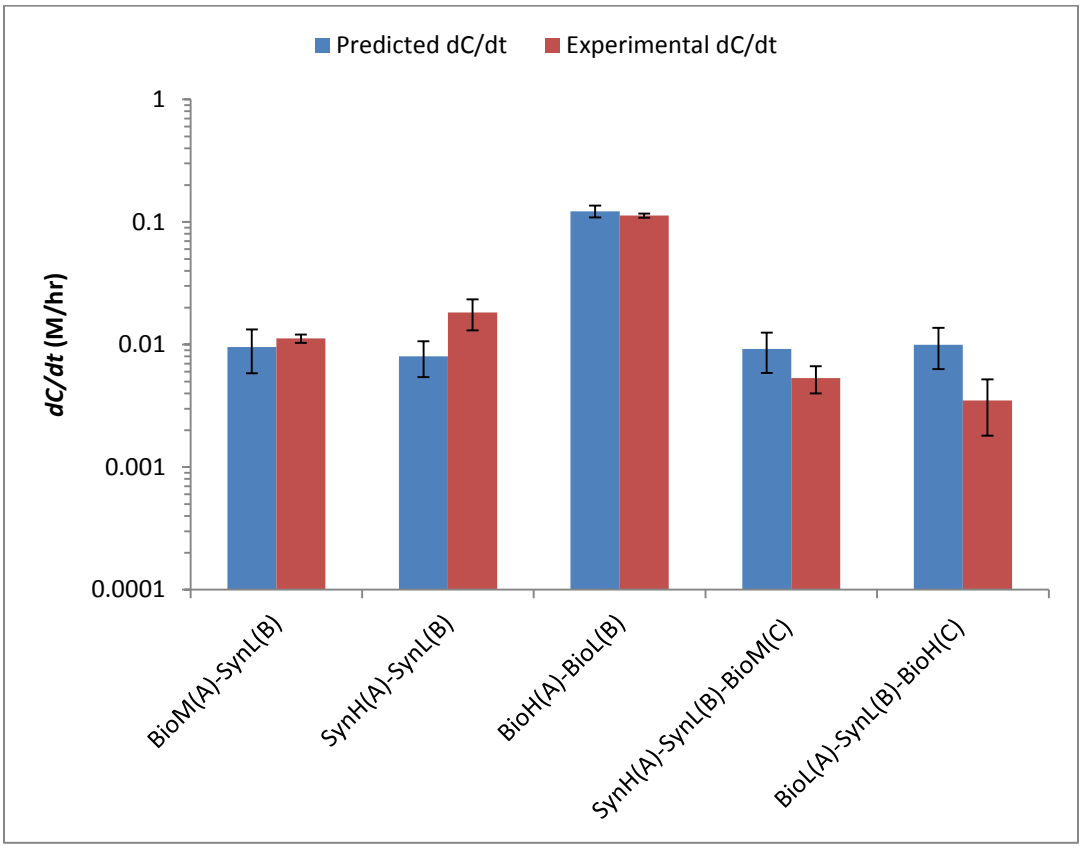

Figure 43. Predicted and experimental permeation rate (*dC/dt*) of overall multi-phase nanocomposite films with various combinations of nanofilms. All error bars indicate 95% confidence interval (n=3).

6.4. Conclusions

Integrating multi-phase nanofilms based on known properties of individual bi-component films were investigated by theoretical predictions and experimental measurements.

To our knowledge, no modeling method has been proposed to match experimental data of this kind. Our statistical analysis reveals that the worst errors are within an order of magnitude of the actual values. Thus, it could be used reasonably well as a predication tool for design of multi-phase nanocomposite films.

7. CONCLUSIONS

We were successful in achieving five aims: (1) exploring the diffusion of target analytes through self-assembled, nanoscale multilayer films and correlating this with the film composition; (2) advancing biosensor development by applying improved transport-limiting membranes to sensor systems; (3) modifying diffusion-limiting film surfaces with protein-resistance; (4) expanding the material selection in biological polymers such as natural materials, polypeptides, and polysaccharides; and (5) integrating multi-phase nanocomposite films based on known properties of individual components.

The specific architectures of the various nanofilms determined the transport properties of target molecules such as glucose, urea, and lactate, since permeability values of the nanofilms were strongly influenced by the composition of the films and the size of target molecules rather than the charge of the molecule. Nanofilm coatings around 100nm thickness decreased diffusion coefficients of small molecules up to five orders of magnitude. These results suggest nanofilms can be used as a general strategy, tailored to match the transport requirements of biosensors measuring different target analytes.

The presence of salt during deposition of diffusion-limiting nanofilms was found to greatly affect glucose permeation and, consequently, sensor response. The decreased glucose diffusion results in decreased sensitivity and increased range of sensor response. Our findings also suggest that careful analysis of materials is required to reveal potential problems for *in vivo* biosensor coating applications to provide multi-function. Along

with the desired diffusion control, susceptibility of underlying multilayers to environmental influence must be considered. It was revealed that weak-weak PEMs should not be used to control transport due to their irregular behavior under normal physiological conditions, even though they offer superior diffusion resistance.

Application of a terminal layer of protein-resistant material does not substantially affect total film permeability. Despite the lower permeability to glucose compared to strong-weak films, weak-weak films exhibited large variation in permeability after protein exposure, even when PEG surface coatings were applied. In contrast, strong-weak pairs were more robust and maintained stable diffusion control when exposed to proteins. Thus, multilayers of strong-weak pairs should be used to achieve and maintain the desired flux balance, which may require deposition of thicker layers to obtain lower permeability.

We investigated construction of biological polyelectrolyte multilayers (BPEMs) at the nanometer scale in a physiological environment, and determined diffusion properties of glucose through each BPEM. Diffusivity of glucose through all the BPEMs, including native and crosslinked films, was three to four orders of magnitude lower than the D value of bare substrate in all cases. Permeation rates (dC/dt) of all BPEMs were up to two orders of magnitude higher than the [PAA/PAH]-based film. Crosslinked BPEMs decreased diffusivity of glucose up to 51% as compared to native BPEMs. The fundamental properties for a biomedical device coating that maximizes biomimetic properties at the interface while ensuring diffusion-limited behavior over the range of interest can be applied in drug delivery, cell systems, and tissue engineering.

The outcomes from this work will be the key knowledge or engineering principles to support future efforts in research and development. It is anticipated that the automated system developed for determining transport properties will provide a general platform for assessing new candidate materials. The theory developed will be useful in estimating transport properties of novel nanocomposite materials that may be interesting in a broad array of chemical and biological systems, from analytical separations to biomedical applications, and will provide useful design rules for materials and fabrication process selection.

For future work, specific applications for nanofilm coatings can be followed by *in vivo* clinical studies of phenomena such as biodegradation, biostability, and biofouling. As discussed in Section 6, PAA/PAH possesses great transport-limiting properties for small molecules. However, its transport properties are altered in the physiological environment. Thus, stability of PAA/PAH is an important issue for *in vivo* applications. Crosslinking of PAA/PAH might be an option to enhance the stability of the film, and it requires investigation of diffusion studies of protein and serum adsorption (as discussed in Section 4) with crosslinked PAA/PAH films.

In future studies, other materials could be considered. As an example, poly(diallyldimethylammonium chloride), PDADMAC, is a polycation like PAH. PDADMAC is a strong polyelectrolyte, while PAH is pH-sensitive. Properties of multilayers comprised of PDADMAC and PSS will differ greatly from those comprised of PAH and PSS. For example, PSS/PDADMAC is more easily swollen[108] than PSS/PAH, whereas PSS/PAH has a much higher modulus[109] and provides a much

greater barrier to ion transport.[110, 111] Another consideration of materials is hyaluronic acid (HA), a major component of extracellular matrix. It is implicated in joint lubrication, water homeostasis of tissues cell motility and inflammation.[112, 113] HA is a linear, unbranched, fully biodegradable and biocompatible polyanion. HA has been incorporated into LbL multilayers in conjunction with many synthetic or biological polymers such as PAH,[114] PLL,[115] heparin,[116] chitosan,[117] and collagen.[95] These materials are fully compatible with the LbL process, and will provide a wide variety of uses for functional nanofilm coatings.

REFERENCES

(1) Gough, D. A.; Lucisano, J. Y.; Tse, P. H. S. *Anal. Chem.* **1985**, *57*, 2351-2357.

(2) Ladam, G.; Schaaf, P.; Decher, G.; Voegel, J.-C.; Cuisinier, F. J. G. *Biomol. Eng.* **2002**, *19*, 273-280.

(3) Anderson, J. M. In *Biomaterials Science*, 1st ed.; Ratner, B., Hoffman, A., Schoen, F., Lemons, J., Eds.; Academic Press: **1996**; Vol. 1. 165-173.

(4) *Multilayer Thin Films: Sequential Assembly of Nanocomposite Materials* 1st ed.; Decher, G.; Schlenoff, J. B., Eds.; Wiley-VCH: **2003**; 543.

(5) Decher, G.; Lvov, Y.; Schmitt, J. *Thin Solid Films* **1994**, *244*, 772-777.

(6) Decher, G. *Science* **1997**, *277*, 1232-1237.

(7) Lvov Yu, M.; Sukhorukov, G. B. *Membr. Cell Biol.* **1997**, *11*, 277-303.

(8) Sano, M.; Lvov, Y.; Kunitake, T. *Annu. Rev. Mater. Sci.* **1996**, *26*, 153-187.

(9) Lvov, Y.; Ariga, K.; Onda, M.; Ichinose, I.; Kunitake, T. *Langmuir* **1997**, *13*, 6195-6203.

(10) Lvov, Y.; Ariga, K.; Ichinose, I.; Kunitake, T. *J. Am. Chem. Soc.* **1995**, *117*, 6117-6123.

(11) Keller, S. W.; Kim, H.-N.; Mallouk, T. E. *J. Am. Chem. Soc.* **1994**, *116*, 8817-8818.

(12) Kotov, N. A.; Dekany, I.; Fendler, J. H. *J. Phys. Chem.* **1995**, *99*, 13065-13069.

(13) Schüler, C.; Caruso, F. *Macromol. Rapid Commun.* **2000**, *21*, 750-753.

(14) Anzai, J.-i.; Takeshita, H.; Kobayashi, Y.; Osa, T.; Hoshi, T. *Anal. Chem.* **1998**, *70*, 811-817.

(15) Hoshi, T.; Saiki, H.; Kuwazawa, S.; Tsuchiya, C.; Chen, Q.; Anzai, J. i. *Anal. Chem.* **2001**, *73*, 5310-5315.

(16) Lvov, Y.; Antipov, A. A.; Mamedov, A.; Möhwald, H.; Sukhorukov, G. B. *Nano Lett.* **2001**, *1*, 125-128.

(17) Wilson, R.; Turner, A. P. F. *Biosens. Bioelectron.* **1992**, *7*, 165-185.

(18) Bremer, T. M.; Edelman, S. V.; Gough, D. A. *Diabetes Technol. Ther.* **2001**, *3*, 409-418.

(19) Stucker, M.; Struk, A.; Altmeyer, P.; Herde, M.; Baumgartl, H.; Lubbers, D. W. *J. Physiol.* **2002**, *538*, 985-994.

(20) Evans, N. T.; Naylor, P. F. *Respir. Physiol.* **1966**, *2*, 61-72.

(21) Wu, C.-C.; Yasukawa, T.; Shiku, H.; Matsue, T. *Sens. Actuators, B* **2005**, *110*, 342-349.

(22) Rego, R.; Caetano, N.; Vale, R.; Mendes, A. *J. Membr. Sci.* **2004**, *244*, 35-44.

(23) Rivera, H.; Cole, A.; Santiago-Aviles, J.; Smith, D. *Sensors* **1994**, *11*, 72-73.

(24) Salimi, A.; Roushani, M. *Electrochem. Commun.* **2005**, *7*, 879-887.

(25) Zhang, Y.; Hu, Y.; Wilson, G. S.; Moatti-Sirat, D.; Poitout, V.; Reach, G. *Anal. Chem.* **1994**, *66*, 1183-1188.

(26) Lu, J.; Do, I.; Drzal, L. T.; Worden, R. M.; Lee, I. *ACS Nano* **2008**, *2*, 1825-1832.

(27) Desai, T. A.; Hansford, D. J.; Leoni, L.; Essenpreis, M.; Ferrari, M. *Biosens. Bioelectron.* **2000**, *15*, 453-462.

(28) Uehara, H.; Kakiage, M.; Sekiya, M.; Sakuma, D.; Yamonobe, T.; Takano, N.; Barraud, A.; Meurville, E.; Ryser, P. *ACS Nano* **2009**, *3*, 924-932.

(29) Liu, X.; Bruening, M. L. **2004**, *16*, 351-357.

(30) Miller, M. D.; Bruening, M. L. *Langmuir* **2004**, *20*, 11545-11551.

(31) Harris, J. J.; Stair, J. L.; Bruening, M. L. *Chem. Mater.* **2000**, *12*, 1941-1946.

(32) Stein, E. W.; Grant, P. S.; Zhu, H.; McShane, M. J. *Anal. Chem.* **2007**, *79*, 1339-1348.

(33) Stein, E. W.; Singh, S.; McShane, M. J. *Anal. Chem.* **2008**, *80*, 1408-1417.

(34) Zhao, W.; Xu, J. J.; Chen, H. Y. *Electroanalysis* **2006**, *18*, 1737-1748.

(35) Lutkenhaus, J. L.; Hammond, P. T. *Soft Matter* **2007**, *3*, 804-816.

(36) Gregor, H. P.; Luttinger, L. B.; Loebl, E. M. *J. Phys. Chem.* **1955**, *59*, 34-39.

(37) Bhatia, S. R.; Khattak, S. F.; Roberts, S. C. *Curr. Opin. Colloid Interface Sci.* **2005**, *10*, 45-51.

(38) Raabo, E.; Terkildsen, T. C. *Scand. J. Clin. Lab. Invest.* **1960**, *12*, 402 - 407.

(39) In *Transport Phenomena in Biological Systems*, 1st ed.; Truskey, G. A., Yuan, F., Katz, D. F., Eds.; Pearson Prentice Hall: Upper Saddle River, N.J., **2004**; p 257-330.

(40) Mendelsohn, J. D.; Barrett, C. J.; Chan, V. V.; Pal, A. J.; Mayes, A. M.; Rubner, M. F. *Langmuir* **2000**, *16*, 5017-5023.

(41) Fery, A.; Scholer, B.; Cassagneau, T.; Caruso, F. *Langmuir* **2001**, *17*, 3779-3783.

(42) Hiller, J. A.; Mendelsohn, J. D.; Rubner, M. F. *Nat. Mater.* **2002**, *1*, 59-63.

(43) Zhai, L.; Nolte, A. J.; Cohen, R. E.; Rubner, M. F. *Macromolecules* **2004**, *37*, 6113-6123.

(44) Schultz, S. G.; Solomon, A. K. *J. Gen. Physiol.* **1961**, *44*, 1189-1199.

(45) Bouchoux, A.; Balmann, H. R.-d.; Lutin, F. *J. Membr. Sci.* **2005**, *258*, 123-132.

(46) Bowen, W. R.; Mohammad, A. W.; Hilal, N. *J. Membr. Sci.* **1997**, *126*, 91-105.

(47) Borisov, S. M.; Wolfbeis, O. S. **2008**, *108*, 423-461.

(48) Ronkainen, N. J.; Halsall, H. B.; Heineman, W. R. **2010**, *39*, 1747-1763.

(49) Wilson, G. S.; Gifford, R. **2005**, *20*, 2388-2403.

(50) Singh, S.; McShane, M. *Biosens. Bioelectron.* **2010**, *25*, 1075-1081.

(51) Schlenoff, J. B.; Ly, H.; Li, M. *J. Am. Chem. Soc.* **1998**, *120*, 7626-7634.

(52) Dubas, S. T.; Schlenoff, J. B. *Macromolecules* **1999**, *32*, 8153-8160.

(53) Farhat, T. R.; Schlenoff, J. B. *Langmuir* **2001**, *17*, 1184-1192.

(54) Jiang, C.; Wang, X.; Gunawidjaja, R.; Lin, Y.-H.; Gupta, M. K.; Kaplan, D. L.; Naik, R. R.; Tsukruk, V. V. *Adv. Funct. Mater.* **2007**, *17*, 2229-2237.

(55) Battle, A. R.; Valenzuela, S. M.; Mechler, A.; Nichols, R. J.; Praporski, S.; di Maio, I. L.; Islam, H.; Girard-Egrot, A. P.; Cornell, B. A.; Prashar, J.; Caruso, F.; Martin, L. L.; Martin, D. K. *Adv. Funct. Mater.* **2009**, *19*, 201-208.

(56) Zhang, X.; Sharma, K. K.; Boeglin, M.; Ogier, J.; Mainard, D.; Voegel, J.-C.; Meəly, Y.; Benkirane-Jessel, N. *Nano Lett.* **2008**, *8*, 2432-2436.

(57) Volodkin, D.; Arntz, Y.; Schaaf, P.; Moehwald, H.; Voegel, J.-C.; Ball, V. *Soft Matter* **2008**, *4*, 122-130.

(58) Swiston, A. J.; Cheng, C.; Um, S. H.; Irvine, D. J.; Cohen, R. E.; Rubner, M. F. *Nano Lett.* **2008**, *8*, 4446-4453.

(59) Guillaume-Gentil, O.; Akiyama, Y.; Schuler, M.; Tang, C.; Textor, M.; Yamato, M.; Okano, T.; Vörös, J. *Adv. Mater.* **2008**, *20*, 560-565.

(60) Berthelemy, N.; Kerdjoudj, H.; Gaucher, C.; Schaaf, P.; Stoltz, J.-F.; Lacolley, P.; Voegel, J.-C.; Menu, P. *Adv. Mater.* **2008**, *20*, 2674-2678.

(61) Jeon, S. I.; Lee, J. H.; Andrade, J. D.; De Gennes, P. G. *J. Colloid Interface Sci.* **1991**, *142*, 149-158.

(62) Lutkenhaus, J. L.; Olivetti, E. A.; Verploegen, E. A.; Cord, B. M.; Sadoway, D. R.; Hammond, P. T. *Langmuir* **2007**, *23*, 8515-8521.

(63) Zahr, A. S.; Davis, C. A.; Pishko, M. V. *Langmuir* **2006**, *22*, 8178-8185.

(64) Heuberger, R.; Sukhorukov, G.; Vörös, J.; Textor, M.; Möhwald, H. *Adv. Funct. Mater.* **2005**, *15*, 357-366.

(65) Pasche, S.; DePaul, S. M.; Voros, J.; Spencer, N. D.; Textor, M. *Langmuir* **2003**, *19*, 9216-9225.

(66) Elbert, D. L.; Hubbell, J. A. *Chem. Biol.* **1998**, *5*, 177-183.

(67) Michel, R.; Pasche, S.; Textor, M.; Castner, D. G. *Langmuir* **2005**, *21*, 12327-12332.

(68) Huang, N.-P.; Michel, R.; Voros, J.; Textor, M.; Hofer, R.; Rossi, A.; Elbert, D. L.; Hubbell, J. A.; Spencer, N. D. *Langmuir* **2001**, *17*, 489-498.

(69) Jeon, J.; Panchagnula, V.; Pan, J.; Dobrynin, A. V. *Langmuir* **2006**, *22*, 4629-4637.

(70) Kato, N.; Schuetz, P.; Fery, A.; Caruso, F. *Macromolecules* **2002**, *35*, 9780-9787.

(71) Balachandra, A. M.; Dai, J.; Bruening, M. L. *Macromolecules* **2002**, *35*, 3171-3178.

(72) Schuetz, P.; Caruso, F. *Adv. Funct. Mater.* **2003**, *13*, 929-937.

(73) Sauerbrey, G. *Z. Phys. A: Hadrons Nucl.* **1959**, *155*, 206-222.

(74) Chen, H.; Hu, X.; Zhang, Y.; Li, D.; Wu, Z.; Zhang, T. *Colloids Surf., B* **2008**, *61*, 237-243.

(75) Ladam, G.; Gergely, C.; Senger, B.; Decher, G.; Voegel, J.-C.; Schaaf, P.; Cuisinier, F. J. G. *Biomacromolecules* **2000**, *1*, 674-687.

(76) Salloum, D. S.; Schlenoff, J. B. *Biomacromolecules* **2004**, *5*, 1089-1096.

(77) Shiratori, S. S.; Rubner, M. F. *Macromolecules* **2000**, *33*, 4213-4219.

(78) Tanchak, O. M.; Barrett, C. J. *Chem. Mater.* **2004**, *16*, 2734-2739.

(79) Gergely, C.; Bahi, S.; Szalontai, B.; Flores, H.; Schaaf, P.; Voegel, J.-C.; Cuisinier, F. J. G. *Langmuir* **2004**, *20*, 5575-5582.

(80) Tang, L.; Thevenot, P.; Hu, W. *Curr. Top. Med. Chem.* **2008**, *8*, 270-280.

(81) Gerritsen, M.; Jansen, J. A.; Lutterman, J. A. *Netherlands J. Med.* **1999**, *54*, 167-179.

(82) Koppolu, B.; Rahimi, M.; Nattama, S.; Wadajkar, A.; Nguyen, K. T. *Nanomed.-Nanotechnol.* **2010**, *6*, 355-361.

(83) Wang, C.; Ye, W.; Zheng, Y.; Liu, X.; Tong, Z. *Int. J. Pharm.* **2007**, *338*, 165-173.

(84) Tang, Z.; Wang, Y.; Podsiadlo, P.; Kotov, N. A. *Adv. Mater.* **2006**, *18*, 3203-3224.

(85) Boudou, T.; Crouzier, T.; Ren, K.; Blin, G.; Picart, C. *Adv. Mater.* **2010**, *22*, 441-467.

(86) Richert, L.; Boulmedais, F.; Lavalle, P.; Mutterer, J.; Ferreux, E.; Decher, G.; Schaaf, P.; Voegel, J.-C.; Picart, C. *Biomacromolecules* **2004**, *5*, 284-294.

(87) Elbert, D. L.; Herbert, C. B.; Hubbell, J. A. *Langmuir* **1999**, *15*, 5355-5362.

(88) Lavalle, P.; Gergely, C.; Cuisinier, F. J. G.; Decher, G.; Schaaf, P.; Voegel, J. C.; Picart, C. *Macromolecules* **2002**, *35*, 4458-4465.

(89) Dai, J.; Jensen, A. W.; Mohanty, D. K.; Erndt, J.; Bruening, M. L. *Langmuir* **2001**, *17*, 931-937.

(90) Liu, H.; Faucher, K. M.; Sun, X.-L.; Feng, J.; Johnson, T. L.; Orban, J. M.; Apkarian, R. P.; Dluhy, R. A.; Chaikof, E. L. *Langmuir* **2002**, *18*, 1332-1339.

(91) Maurstad, G.; Mørch, Y. A.; Bausch, A. R.; Stokke, B. T. *Carbohydr. Polym.* **2008**, *71*, 672-681.

(92) Alves, N. M.; Picart, C.; Mano, J. F. *Macromol. Biosci.* **2009**, *9*, 776-785.

(93) Glinel, K.; Prevot, M.; Krustev, R.; Sukhorukov, G. B.; Jonas, A. M.; Mohwald, H. *Langmuir* **2004**, *20*, 4898-4902.

(94) Schneider, A.; Vodouhê, C.; Richert, L.; Francius, G.; Le Guen, E.; Schaaf, P.; Voegel, J.-C.; Frisch, B.; Picart, C. *Biomacromolecules* **2006**, *8*, 139-145.

(95) Johansson, J. A.; Halthur, T.; Herranen, M.; Soderberg, L.; Elofsson, U.; Hilborn, J. *Biomacromolecules* **2005**, *6*, 1353-1359.

(96) Etienne, O.; Schneider, A.; Taddei, C.; Richert, L.; Schaaf, P.; Voegel, J.-C.; Egles, C.; Picart, C. *Biomacromolecules* **2005**, *6*, 726-733.

(97) Collin, D.; Lavalle, P.; Garza, J. M.; Voegel, J.-C.; Schaaf, P.; Martinoty, P. *Macromolecules* **2004**, *37*, 10195-10198.

(98) Boulmedais, F.; Bozonnet, M.; Schwinte, P.; Voegel, J. C.; Schaaf, P. *Langmuir* **2003**, *19*, 9873-9882.

(99) Pilbat, A. M.; Ball, V.; Schaaf, P.; Voegel, J. C.; Szalontai, B. *Langmuir* **2006**, *22*, 5753-5759.

(100) Boudou, T. rouzier, T. Auz ly-Velty, R.; Glinel, K.; Picart, C. *Langmuir* **2009**, *25*, 13809-13819.

(101) Park, J.; McShane, M. J. *ACS Appl. Mater. Interfaces* **2010**, *2*, 991-997.

(102) Wang, G.; Zhou, J. H.; Li, J. H. *Biosens. Bioelectron.* **2007**, *22*, 2921-2925.

(103) Manna, U.; Patil, S. *Langmuir* **2009**, *25*, 10515-10522.

(104) Jean, B.; Heux, L.; Dubreuil, F.; Chambat, G.; Cousin, F. *Langmuir* **2009**, *25*, 3920-3923.

(105) Schmidt, D. J.; Cebeci, F. C.; Kalcioglu, Z. I.; Wyman, S. G.; Ortiz, C.; Van Vliet, K. J.; Hammond, P. T. *ACS Nano* **2009**, *3*, 2207-2216.

(106) Ouyang, L.; Malaisamy, R.; Bruening, M. L. *J. Membr. Sci.* **2008**, *310*, 76-84.

(107) Schadler, L. S. In *Nanocomposite Science and Technology*, Eds.; Wiley-VCH Verlag GmbH & Co. KGaA: 2004; 77-153.

(108) Dubas, S. T.; Schlenoff, J. B. *Langmuir* **2001**, *17*, 7725-7727.

(109) Nolte, A. J.; Rubner, M. F.; Cohen, R. E. *Macromolecules* **2005**, *38*, 5367-5370.

(110) Harris, J. J.; Bruening, M. L. *Langmuir* **2000**, *16*, 2006-2013.

(111) Jaber, J. A.; Schlenoff, J. B. *Langmuir* **2007**, *23*, 896-901.

(112) Lap k, L. Lap k, L. De Smedt, S. Demeester, . habre ek, P. *Chem. Rev.* **1998**, *98*, 2663-2684.

(113) Zhang, J.; Senger, B.; Vautier, D.; Picart, C.; Schaaf, P.; Voegel, J.-C.; Lavalle, P. **2005**, *26*, 3353-3361.

(114) Szarpak, A.; Cui, D.; Dubreuil, F.; De Geest, B. G.; De Cock, L. J.; Picart, C.; Auzely-Velty, R. **2010**, *11*, 713-720.

(115) Picart, C.; Lavalle, P.; Hubert, P.; Cuisinier, F. J. G.; Decher, G.; Schaaf, P.; Voegel, J.-C. *Langmuir* **2001**, *17*, 7414-7424.

(116) Huang, L. Y.; Yang, M. C. *J. Nanosci. Nanotechno.* **2006**, *6*, 3163-3170.

(117) Bongaerts, J. H. H.; Cooper-White, J. J.; Stokes, J. R. *Biomacromolecules* **2009**, *10*, 1287-1294.

APPENDIX A

Experimental description of luminescent glucose sensor test* described in Section 3.

Materials

Unless stated otherwise, chemicals were obtained from Sigma. Porous, amine-modified silica microspheres (YM Amer ica, Inc., 10.3 μm average diameter, 13.1 nm average pore diameter) were used as the sensor substrate. Carboxyl-amine coupling was performed using N-(3-dimethylaminopropyl)-N′-ethylcarbodiimide hydrochloride (EDC) and N-hydroxysulfosuccinimide sodium salt (sulfo-NHS, Toronto Research Chemicals Inc.). Palladium(II) meso-Tetra(4-carboxyphenyl) porphine (PdP, Frontier Scientific) and glucose oxidase (GOx, EC 232-601-0) were used to make glucose sensors. The dye was initially dissolved in dimethyl sulfoxide (DMSO). Potassium phosphate was used to create a buffer for carboxyl-amine coupling. Poly(allylamine hydrochloride) (PAH, MW 70 kDA), poly(sodium 4-styrenesulfonate) (PSS, MW 70 kDA), and sodium chloride were used during the deposition of nanofilms. A Sylgard 184 silicone elastomer kit (Dow Corning) was used to create polydimethylsiloxane (PDMS) molds. Gels were used to immobilize sensor particles and were prepared by mixing poly(ethylene glycol) monomethyl ether monomethacrylate (PEG, 1000 MW,

---

* Adopted from Collier, B.; Park, J.; McShane, M. *2010 IEEE Sensors* **2010**, 1587-1591.

Polysciences) and DI water. A solution consisting of Irgacure 184 (Ciba) dissolved in DMSO was used as an initiator for gel cross-linking. A silanol solution consisting of anhydrous ethanol DI water, and 3-(trimethoxysilyl)propyl methacrylate was used to attach the PEG gel to a glass slide. Phosphate buffered saline (PBS) solution was prepared using sodium phosphate monobasic (2.7 mM), sodium phosphate dibasic (7.7 mM), and sodium chloride (154 mM). Solutions of D-(+)-glucose were made from PBS and compressed air was diffused into buffer solutions during dynamic testing. All necessary pH adjustments were performed using titrations of 1.0 M HCl and 1.0 M NaOH. All chemicals listed above were reagent grade and used as received. Ultrapure water with a resistivity of 18.2 MΩ-cm was used to prepare all aqueous solutions.

Sensor Preparation

Initially, 100 mg of microspheres, 20 mg of EDC, and 23 mg of sulfo-NHS were dissolved in 1 mL of potassium phosphate buffer (0.1 M, pH 7). Then 200 μL of PdP solution (1.5 mM in DMSO) was added to the solution and vortexed at low speeds. After 1 hr, the solution was rinsed and the supernatant removed. A solution of 20 mg of EDC and 23 mg of sulfo-NHS was again added in 1 mL of phosphate buffer and vortexed at low speeds for 20 minutes. After rinsing the particles and removing the supernatant, 0.9 mL of GOx solution (20 mg/mL phosphate buffer) was added and vortexed at low speeds for 2 hrs. After rinsing, nanofilms were deposited on the glucose sensors using the layer-by-layer technique.[32, 33, 50] PSS and PAH (0.02 M, pH 5) were alternately

exposed to the sensors with various salt concentrations until 15 bilayers were constructed.

A PDMS mold was created by mixing silicone elastomer base and silicone elastomer curing agent in a ratio of 9:1 (v/v). After mixing and placing in a petri dish, the elastomer was placed under vacuum for 20 minutes to remove any bubbles and then immediately placed in an oven at 75° C for 2 hrs. The resulting PDMS was cut up into smaller pieces (~1 cm^2) and a biopsy punch was used to make a hole in the center of the new pieces. A glass slide and the new mold were treated with a Laboratory Corona Treater (Electro-Technic Products, Inc., Model BD-20AC) to facilitate binding. Pressure was then applied to the mold for two hours to ensure secure bonding. After creating a silane solution, 1 μL was added to the glass slide in the hole formed by the PDMS mold. After allowing drying under ambient room conditions, the silanized spot was rinsed with pure ethanol and again allowed to dry.

Initially, 40 μL of sensor solution was centrifuged and the supernatant was removed. Then 10 μL of PEG solution (1.4 g/mL) and 0.5 μL of Irgacure solution (20 mg/mL DMSO) were added. After briefly vortexing, 7 μL of the solution was placed on a silanized glass slide in a post-shaped PDMS mold and cured under UV light for 10 minutes. This allows reaction of acrylate groups on the glass slide with acrylate groups present on the PEG. After exposure, the mold was removed and the gel was placed inside a custom reaction chamber allowing PBS buffer to flow over the sensor gel.[50] After sufficient swelling time (i.e., > 1 hr) to allow stabilization of the luminescent signal, the response of the sensors was tested.

A mass flow controller (MFC, type 1179A, MKS Instruments) and a 2 channel power supply and readout (PR4000, MKS Instruments) were used to diffuse compressed air in buffer and glucose solution reservoirs. Solutions from these reservoirs were mixed using two peristaltic pumps (Masterflex, Model 7550-50) to expose sensors to the desired glucose concentration.[50] A multi-frequency phase fluorometer (TauTheta Instruments, LLC, MFPF-100) was then used to drive LED excitation of the sensors at 1 kHz and obtain luminescence lifetime measurements. A custom virtual instrument software program (LabVIEW, National Instruments) was used to provide overall system control.

Sensor Testing

Initially gels were exposed to a randomized set of glucose concentrations while the lifetime response was recorded. Three separate gels were tested for each set of sensors made with different salt concentrations. The lifetime response was converted to percent change relative to the baseline glucose response at 0 mg/dL. The steady state responses from each concentration were averaged for each individual test. The results from three tests of different sensors were used to find an average and a standard deviation for the overall sensor response.

VITA

Name: Jae Bum Park

Address: 5045 Emerging Technologies Building

3120 TAMU

College Station, TX 77843-3120

Email Address: jbagst@hotmail.com

Education: B.S., Chemistry, Hallym University, 2000

M.S., Chemistry, Hallym University, 2002

Ph.D. Materials Science and Engineering, Texas A&M University, 2012